CHALMERS

Prospects for dark matter detection with next generation neutrino telescopes

MSc thesis in Physics and Astronomy

ANTON BÄCKSTRÖM

Department of Physics
CHALMERS UNIVERSITY OF TECHNOLOGY
Göteborg 2018

Masters thesis 2018:

Prospects for dark matter detection with next generation neutrino telescopes

ANTON BÄCKSTRÖM

CHALMERS

Department of Physics
Chalmers University of Technology
Göteborg 2018

Prospects for dark matter detection with next generation neutrino telescopes
ANTON BÄCKSTRÖM

Supervisor: Riccardo Catena, Department of Physics
Examiner: Ulf Gran, Department of Physics

Department of Physics
Chalmers University of Technology
SE-412 96 Göteborg
Telephone +46 31 772 1000

Typeset in LaTeX
Printed by Chalmers reproservice
Göteborg, 2018

Prospects for dark matter detection with next generation neutrino telescopes
ANTON BÄCKSTRÖM
Department of Physics
Chalmers University of Technology

Abstract

There are strong hints that around a fourth of the energy content of the Universe is made up of dark matter. This type of matter is invisible to us, since it does not interact via the electromagnetic force. One of the leading theories suggests that this type of matter consists of Weakly Interacting Massive Particles (WIMPs), particles with mass around 10-1000 GeV that only interact with baryonic matter via the weak nuclear force and gravitation. If this theory is true, dark matter should be gravitationally attracted toward the Sun, inside which collisions with baryonic matter have a possibility to slow down the particles to speeds below the escape velocity. As these dark matter particles are captured by the Sun, they will continue to collide with baryonic particles and lose more energy until they settle in the core of the Sun. When the concentration of dark matter particles is sufficiently high in the core, they will self-annihilate with each other, resulting in the creation of Standard Model particles which eventually will decay into neutrinos. These neutrinos will escape the Sun and can possibly be detected in a neutrino telescope. One such telescope is IceCube located at the South Pole, consisting of detectors placed in a cubic kilometer of ice. There is a plan to upgrade this telescope which is called Precision IceCube Next Generation Upgrade (PINGU). In my thesis I have investigated the sensitivity of PINGU to the strength of interactions between dark matter and baryonic matter.

The analysis have been performed for the 28 lowest order operators in a non-relativistic effective field theory for a dark matter particle with spin half, annihilating into either $b\bar{b}$ or $\tau\bar{\tau}$ which decays into ν_μ and $\bar{\nu_\mu}$. I have found that PINGU will improve current IceCube exclusion limits on the coupling constant of the theory for a dark matter mass less than 100 GeV for the $b\bar{b}$ channel and less than ~ 40 GeV for the $\tau\bar{\tau}$ channel, after just one year of data taking, for all 28 operators.

Thanks to

It is my pleasure to thank my supervisor Riccardo Catena for this opportunity. I would also like to thank Kåre Fridell, Fredrik Hellström, Martin Krauss and Vanessa Zema for helping me learn more about dark matter. Finally I would like to thank Carlos Pérez de los Heros of the IceCube collaboration for important insights regarding the IceCube detectors.

Anton Bäckström
Göteborg, 2018

Contents

1 Introduction **1**

2 Theory **3**

2.1 An overview of astrophysics and cosmology . . . 3
2.1.1 The geometry of the Universe . . . 3
2.1.2 The content of the Universe . . . 4
2.1.3 The history of the Universe . . . 5
2.1.3.1 The Planck era ($< 10^{-43}$ s) . . . 5
2.1.3.2 The grand unification era ($10^{-43} - 10^{-36}$ s) . . . 5
2.1.3.3 The electroweak era ($10^{-36} - 10^{-12}$ s): the inflationary era ($10^{-36} - \sim 10^{-33}$ s) and the reheating era ($\sim 10^{-33} - 10^{-12}$ s) . . . 5
2.1.3.4 The quark era ($10^{-12} - 10^{-6}$ s) . . . 5
2.1.3.5 The hadron era ($10^{-6} - 1$ s) . . . 6
2.1.3.6 The lepton era ($1 - 10$ s) . . . 6
2.1.3.7 Nucleosynthesis ($3 - 20$ min) . . . 6
2.1.3.8 Matter domination (70000 years) . . . 6
2.1.3.9 Recombination (380000 years) . . . 6
2.1.3.10 Structure formation (150 million years onward) . . . 6
2.2 Evidence for dark matter . . . 7
2.2.1 Solar neighborhood . . . 7
2.2.2 Galaxy cluster scale . . . 7
2.2.3 Galactic scale . . . 9
2.2.4 Cosmological scale . . . 10
2.3 Solving the dark matter problem . . . 12
2.4 Characteristics of dark matter . . . 12
2.5 Production mechanism . . . 13
2.5.1 Thermal production . . . 13
2.5.2 Non-thermal production . . . 13
2.6 Dark matter particle candidates . . . 14
2.6.1 WIMP . . . 14
2.6.2 Axions . . . 14
2.6.3 Sterile neutrinos . . . 15
2.6.4 Other candidates . . . 15
2.7 Experiments . . . 15

2.7.1 Indirect detection . . . 15
2.7.1.1 Gamma rays . . . 16
2.7.1.2 Cosmic rays . . . 16
2.7.1.3 Neutrinos . . . 16
2.7.2 Direct detection . . . 17
2.7.3 Collider experiments . . . 17
2.8 Effective field theory . . . 18
2.9 The detectors of IceCube . . . 19

3 Method **21**
3.1 WIMP capture by a massive body . . . 21
3.1.1 Simplest case . . . 21
3.1.2 Several particle species and energy-dependent cross section. . . 25
3.1.3 Moving body . . . 26
3.1.4 Including Galactic escape velocity . . . 26
3.1.5 Calculating capture rates . . . 27
3.2 Annihilation rates and neutrino flux . . . 27
3.3 Event rates . . . 28
3.4 Background . . . 28
3.5 Calculation of significance . . . 30
3.6 Astrophysical and experimental input . . . 30

4 Results **33**

5 Discussion **41**
5.1 Uncertainties . . . 41
5.1.1 Astrophysical . . . 41
5.1.2 Experimental . . . 42
5.2 Outlook . . . 42

6 Conclusion **43**

A Appendix: isovector operators **I**

B Appendix: flowchart **VII**

1
Introduction

The world around us is dark. Despite all progress that has been made in physics, the standard model of cosmology tells us that we have investigated objects comprising only about 4.9% of the total energy content of the Universe, whereas the rest is dark to our detection. This hidden part of the Universe consist of 26.8% *dark matter* and 68.3% *dark energy* [1]. This thesis will be focused on the former.

Dark matter has so far only been detected by its interaction with gravity, with observation showing that objects in the universe move too fast for them to be gravitationally bound by the baryonic (or ordinary) matter alone. We also see that structure formation in the Universe would look different in a world without dark matter. Considerable effort is today focused on detecting this elusive form of matter by means other than gravitational, with experiments ranging from indirect detection, direct detection and collider experiments. A review of these will be given in the next chapter. Even though there has been no conclusive detection, these null results puts constraints on how the dark matter particles couple to baryonic matter.

Current cosmological models predict that dark matter forms halos that surrounds galaxies, including our Milky Way. If dark matter consist of some new type of particle, these particles can be gravitationally attracted to the Sun, in which they self-annihilate and produce neutrinos, which can escape the Sun. These neutrinos can possibly be detected by neutrino telescopes, for instance the IceCube Neutrino Observatory located at the South Pole. There is a planned upgrade to this telescope called Precision IceCube Next Generation Upgrade (PINGU) which will be able to detect neutrinos of lower energy than previously possible. This upgrade will either detect dark matter or further constrain the coupling of dark matter to baryonic matter.

The aim of this thesis is to calculate which coupling strength PINGU can probe, given the experimental input in the most general theory of dark matter nucleon interactions, which has not been done before.

Since we do not know how (or if) dark matter interacts with baryonic matter, I will utilize a model independent approach by means of effective field theory. The advantage of such an approach is that we don't need a detailed description of dark matter, rather we look at all possible interactions in a low energy limit.

2

Theory

In this chapter I start by introducing some concepts of cosmology needed to follow the rest of this thesis. I then present the evidence for the presence of dark matter and describe how this evidence can be explained. I continue with a description of the characteristics of dark matter. We then move on to a review of current and upcoming experiments to detect dark matter. This chapter is then concluded with a brief introduction to effective field theory and a discussion about the IceCube observatory. I will use natural units throughout the thesis, $c = 1$ and I will not write out c explicitly in formulas. For example I will write masses in GeV instead of GeV/c^2.

2.1 An overview of astrophysics and cosmology

I assume that the reader have some familiarity with general relativity. I define the metric of flat spacetime with $\eta_{00} = -1,\ \eta_{11} = \eta_{22} = \eta_{33} = 1$.

2.1.1 The geometry of the Universe

The starting point in cosmology is to find a geometric description of our Universe. General relativity tells us that energy curves spacetime. This information is encoded in the metric and from the metric one can construct the line element, which specifies the distance between points (or vice versa).

On scales of the order ~ 100 Mpc (one parsec equals 3.26 light-years $= 3.09 \cdot 10^{16}$ m) the Universe is isotropic and homogeneous, i.e matter is distributed evenly across the sky. We call this the *cosmological principle* and this principle allows three possible spatial line elements, see for instance chapter 14 in Weinberg for a proof of this statement [2]. The first one is the line element of flat space

$$ds^2 = d\mathbf{x}^2, \tag{2.1}$$

where ds is called the proper distance. Next is the line element for a spherical surface of radius a embedded in four dimensional Euclidean space

$$ds^2 = d\mathbf{x}^2 + dz^2, \quad z^2 + \mathbf{x}^2 = a^2, \tag{2.2}$$

this case has a positive curvature. The last possibility is a hyperspherical surface in pseudo-Euclidean space

$$ds^2 = d\mathbf{x}^2 - dz^2, \quad z^2 - \mathbf{x}^2 = a^2, \tag{2.3}$$

where a^2 is some positive constant and this case has a negative curvature. We can combine these three cases into one single line element. We start by rescaling $\mathbf{x}' = a\mathbf{x}$, $z' = az$ and introduce $k = \{-1,0,1\}$, where -1 corresponds to the hyperspherical case, 0 to the flat case, 1 to the spherical case. Dropping primes, the line element can now be written

$$ds^2 = a^2\Big[d\mathbf{x}^2 + k\frac{(\mathbf{x}\cdot d\mathbf{x})^2}{1-k\mathbf{x}^2}\Big]. \tag{2.4}$$

Now we want to extend our spatial line element to spacetime. This is achieved by giving a a time dependence and including dt

$$d\tau^2 \equiv -g_{\mu\nu}dx^\mu dx^\nu = dt^2 - a(t)^2\Big[d\mathbf{x}^2 + k\frac{(\mathbf{x}\cdot d\mathbf{x})^2}{1-k\mathbf{x}^2}\Big], \tag{2.5}$$

where $d\tau$ is called the proper time and $g_{\mu\nu}$ is the metric, in this case the so called *Robertson-Walker* (RW) metric. The scale factor $a(t)$ describes how the scale of the universe changes with time and it is one of the most important quantities in cosmology.

Starting with the RW metric, we would like to know how the Universe evolves. This can be achieved with Einstein's equations, which relates curvature to energy content

$$G_{\mu\nu} + \Lambda g_{\mu\nu} = 8\pi G T_{\mu\nu}, \tag{2.6}$$

where $G_{\mu\nu}$ describes curvature, Λ is a constant responsible for expansion, the so called *dark energy*, G is Newton's constant and $T_{\mu\nu}$ is the stress tensor, which describes the energy content of the Universe. Using the RW metric as input in Einstein's equations and treating the matter/energy as a perfect fluid yields the two equations

$$\frac{\dot{a}+k}{a^2} = \frac{8\pi G\rho + \Lambda}{3}, \tag{2.7}$$

$$\frac{\ddot{a}}{a} = -\frac{4\pi G}{3}(\rho + 3p) + \frac{\Lambda}{3}, \tag{2.8}$$

where dots signify a derivative with respect to time. p is pressure and ρ is density and both of these quantities depend on the scale factor. These two equations constitute the *Friedmann model*.

2.1.2 The content of the Universe

As the Universe expands, the components of the energy density are affected differently by the evolution of the scale factor. For matter $\rho \propto a^{-3}$ and for radiation $\rho \propto a^{-4}$, where the extra factor of a^{-1} is due to the wavelength of the radiation being stretched. Dark energy is not affected by the expansion, this means that it will be important at late cosmological times since the other components thin out.

It is useful to express the energy density of the universe in terms of the critical density $\rho_c = \frac{3H^2}{8\pi G}$, where H is Hubble's parameter, $H \equiv \frac{\dot{a}}{a}$, and G is Newton's gravitational constant. Defining $\Omega_i = \frac{\rho_i}{\rho_c}$, where i is the energy density of either baryonic matter, dark matter, radiation or dark energy gives

$$\Omega = \Omega_b + \Omega_{DM} + \Omega_r + \Omega_\Lambda, \tag{2.9}$$

where b stands for baryonic matter, DM stands for dark matter, r stands for radiation and Λ stands for dark energy. If $\Omega = 1$ the universe is flat, if it is larger than 1 the universe has a positive curvature and is therefore open. $\Omega < 1$ leads to a negative curvature and therefore a closed universe.

2.1.3 The history of the Universe

I will very briefly cover the history of the Universe. The important aspects for this thesis are mainly events during the quark era and onwards, but I include the other eras to put everything into a larger context. I have the divided the history into different eras, specifying the time after the Big Bang in the parenthesis. This section is based on chapter 3 in Mukhanov [3].

2.1.3.1 The Planck era ($< 10^{-43}$ s)

The time before the Planck time 10^{-43} s after the Big Bang is called the Planck era. Little is known about this era. We believe that the Standard Model of particle physics was unified with gravity and that quantum gravity dominated during this time.

2.1.3.2 The grand unification era ($10^{-43} - 10^{-36}$ s)

Following the Planck era, gravity separates from the other fundamental forces, heralding the grand unification era, which lasted until 10^{-36} s. At this point, the strong force separated from the electromagnetic and weak force.

2.1.3.3 The electroweak era (10^{-36}–10^{-12} s): the inflationary era (10^{-36}– $\sim 10^{-33}$ s) and the reheating era ($\sim 10^{-33} - 10^{-12}$ s)

It is possible that the phase transition at the end of the last era might have been the cause of the inflationary process, which ended somewhere between 10^{-33} and 10^{-32} s. This process expanded the volume of the Universe by a factor 10^{78} and repopulated the Universe with quarks and gluons from the decaying inflaton field, we call this the reheating era. Interactions in this quark-gluon soup produced W, Z and Higgs bosons and they continued to be produced until 10^{-12} s, when the universe had become to cold.

2.1.3.4 The quark era ($10^{-12} - 10^{-6}$ s)

The W and Z bosons that were created in the previous era now decayed and the weak force separated from the electromagnetic force and became short-range. The

dark matter abundance is believed to have been frozen-out sometime during either this or the next era.

2.1.3.5 The hadron era ($10^{-6} - 1$ s)

The temperature of the universe is sufficiently cold to allow quarks to bind together and form hadrons, the Quantum ChromoDynamic (QCD) phase transition. Hadrons annihilate with anti-hadrons, but a slight asymmetry between matter and anti-matter result in some hadrons surviving. Neutrinos decouple from photons at the end of this era.

2.1.3.6 The lepton era ($1 - 10$ s)

This era is dominated by leptons and anti-leptons, which are produced until around 10 s after the Big Bang. Leptons and anti-leptons annihilate, but a small fraction of leptons survive due to lepton asymmetry. At this point in time, the energy distribution is dominated by photons.

2.1.3.7 Nucleosynthesis ($3 - 20$ min)

The temperature is low enough for protons to combine into atomic nuclei, forming mainly hydrogen and helium.

2.1.3.8 Matter domination (70000 years)

Now the energy content of the universe consist of equals parts matter and radiation and from this point onward matter will dominate. Structure formation is governed by the so called Jeans length, which specifies the scale which is stable against gravitational collapse. As the Jeans length shrinks, perturbations in the energy density grow larger. This gravitational collapse of inhomogeneities is enhanced by dark matter.

2.1.3.9 Recombination (380000 years)

Electrons are now able to combine with atomic nuclei to form neutral atoms, which is called recombination, in spite of the fact that this is the first time atoms appear in the Universe. Now photons can't remain in thermal equilibrium with matter through scattering with free electrons, which lead to them decoupling from matter, traveling freely. This radiation is called the Cosmic Microwave Background (CMB). Fluctuations in temperature of this nearly perfect black body is important for dark matter, as I will show later on.

2.1.3.10 Structure formation (150 million years onward)

Small inhomogenities in the matter density grow through gravitational instability and form larger and larger structures, eventually giving rise to galaxies.

2.2 Evidence for dark matter

Evidence for dark matter exists on different length and time scales and I will attempt to give a brief overview of this subject.

2.2.1 Solar neighborhood

The earliest mention of a quantitative analysis of dark matter in the Solar neighborhood (SN), a sphere with a radius of about 1kpc $= 3.09 \cdot 10^{16}$, km was carried out by Lord Kelvin in 1904, by describing the stars as particles in a gas and relating their velocity dispersion with mass [4]. He suggests from his observations that 90% of the stars in the SN might be dark or too faint to be detected. Henri Poincaré followed up Kelvin's observations two years later and suggested that the amount of dark matter in the SN is less than the ordinary matter [5]. Similar conclusions were drawn in subsequent observations by Ernst Öpik 1915 and Jacobus Kapteyn 1922 [6] [7]. Kapteyn also came up with a method to determine the local density, by calculating the total gravitational mass and dividing with the amount of stars, through extrapolating the luminosity function. This function relates the number of stars or galaxies per luminosity, which is the energy emitted per unit time. Jan Oort continued this work in 1932 by estimating the density contribution from the luminous matter and dividing the total gravitational mass by the total luminous mass to get the contribution of dark matter [8]. Oort concludes with estimating that dark matter can at most account for half the total matter density in the SN, i.e. $M/M_{lum} \sim 1.1 - 2.0$.

2.2.2 Galaxy cluster scale

The first evidence for dark matter on the Galaxy cluster scale stems from the work of Fritz Zwicky, who in 1933 applied the virial theorem to the Coma cluster [9]. This theorem is a relationship between the potential and kinetic energy of a system,

$$2E_{kin} + E_{pot} = 0 \implies 2\frac{1}{2}M\langle v^2\rangle = \frac{1}{2}\frac{GM^2}{R} \implies M = \frac{2R\langle v^2\rangle}{G}$$

where M is the total mass of the cluster, $\langle v\rangle$ is the average speed of a galaxy, R is the distance from the center of the cluster and G is Newton's gravitational constant. The starting point was to estimate the total mass, which he did by assuming each of the 800 observed galaxies had a mass of 10^9 solar masses, suggested from Hubble. Assuming a size of 10^6 light-years he calculated that the velocity dispersion should be about 80 km/s, which is much less than the observed velocity of about 1000 km/s, suggesting the existence of large amounts of unseen matter.

Zwicky repeated his experiment four years later, this time with the assumption that the Coma cluster consist of 1000 galaxies with a radius of about $2 \cdot 10^6$ light years [10]. This time he used the velocity dispersion as an input in order to get the mass of the cluster. The result was $4.5 \cdot 10^{10}$ solar masses average mass per galaxy. Assuming an absolute luminosity for the cluster of $8.5 \cdot 10^7$ times the luminosity of

the Sun gave a mass to light ratio of about 500. The value of Hubble's constant at that time was $H_0 = 558\text{kms}^{-1}\text{mpc}^{-1}$ compared with todays value of about $H_0 \sim 67$, which show that Zwicky overestimated the mass to light ratio, but the new ratio is still significant. In 1936 Sinclair Smith applied the virial theorem on the Virgo cluster and obtained similar results [11].

People were skeptical about the existence of dark matter however [12][13][14]. There was a hypothesis that galaxy clusters are not bound, which mean that the virial theorem can not be applied to them. This criticism is somewhat justified for the Virgo cluster, since this cluster is irregular and has not reached a stable configuration. On the other hand, the virial theorem should at least approximately apply to the Coma cluster or other spherical or nearly spherical galaxies [15].

Another way to infer the existence of dark matter is through gravitational lensing, which is the effect of light from a background source being bent by matter in the foreground, generating a distorted image of the background source. Gravitational lensing is predicted from both Newton's theory of gravity and general relativity and is classified in three cases: strong lensing, weak lensing and microlensing.

In the strong case, the distortions are easily visible and give rise to arcs. This arc is linked to the amount of mass in the foreground galaxy. In the weak case, the distortions of the background are much smaller and typically a large number of sources need to be analyzed in a statistical way in order to estimate the mass in the foreground. The lensing effect is even smaller in the case of microlensing. Here mass is inferred from changes in the apparent brightness of the source being monitored.

Weak gravitational lensing has been applied to galaxy clusters to infer the existence of dark matter [16]. The most famous example is the galaxy cluster 1E 0657-56, known as the Bullet Cluster which consist of two colliding galaxy clusters [17]. Weak lensing was used in order to map the matter density. This was compared to x-ray measurements which traces the plasma, which is the dominant baryonic matter component.

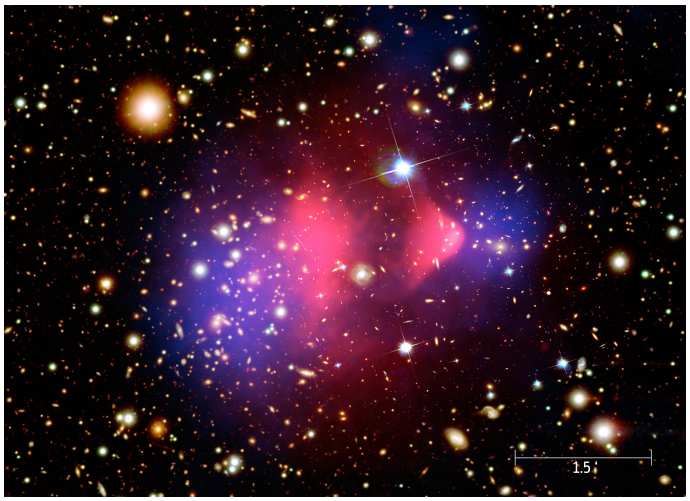

Figure 2.1: *Composite image of the Bullet cluster. The blue part shows the mass distribution calculated via gravitational lensing, the pink part shows the x-ray emission. Figure taken from Wikimedia commons.*

The results show that most of the matter in the clusters just passed through each other without interacting, which is consistent with a dark matter interpretation, while the plasma was trapped in the middle.

2.2.3 Galactic scale

More evidence came in the 70's in the form of rotation curves, which are plots of the radial velocities of stars and gas as a function of the distance from the center of the galaxy.

Consider the distribution of mass in the galaxy to be spherically symmetric. From Newtonian gravity we can balance the gravitational and the centrifugal force acting on some chunk of mass m at a distance r from the galactic center

$$\frac{GmM(r)}{r^2} = \frac{mv(r)^2}{r} \implies v(r) = \sqrt{\frac{GM(r)}{r}},$$

where $v(r)$ is the circular velocity, G is Newton's gravitational constant and $M(r)$ is the enclosed mass at the given radius.

The study of rotation curves was an active research endeavour at this time, with important contributions from Ken Freeman 1970, D. Rogstad and G. Shostak 1972, Morton Roberts and R. Whitehurst 1972, Morton Roberts and Arnold Rots 1973, Nathan Krumm and Edwin Salpeter 1977, Albert Bosma in 1978 [18][19][20][21][22][23]. It all culminated in 1980, when Vera Rubin together with her colleagues Kent Ford and Norbert Thonnard released a paper on rotation curves for 21 spiral galaxies [24].

We expect the velocity to fall as $v(r) \propto r^{-\frac{1}{2}}$, a so called Keplerian orbit, far outside the galactic center, as most of the visible mass is there enclosed, but observations from the researchers mentioned above show instead the behavior $v(r) \propto$ const.. This suggests the existence of unseen matter in a halo outside the visible matter of the galaxy, which scales as $M(r) \propto r$.

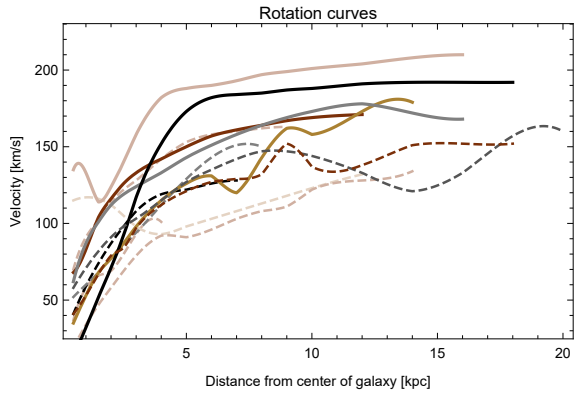

Figure 2.2: *Rotation curves of 15 spiral galaxies. The data is taken from Rubin et al. [24]. All the rotation curves show deviations from the expected $r^{-\frac{1}{2}}$ for large distances r from the center, hinting at unseen matter.*

2.2.4 Cosmological scale

As mentioned in section 2.1.3, the cosmic microwave background (CMB) radiation is a remnant from the early universe when photons became decoupled from matter some 380 000 years after the Big Bang, referred to as the time of last scattering. At this time, the temperature of the universe was around 3000 K, sufficiently cold to allow electrons and protons to combine into atoms [15]. Photons no longer had electrons to scatter off, which is why they decoupled from matter. Since this time, these CMB photons have basically travelled freely and due to the expansion of the universe, they have been been red-shifted by a factor of ~ 1090 [1].

This CMB radiation is close to being a perfect blackbody with a temperature of 2.726 K, with anisotropies of order 10^{-5} [25]. These anisotropies are classified into primary anisotropies, which arose in the early universe, and secondary anisotropies, which arose after the photons decoupled from matter.

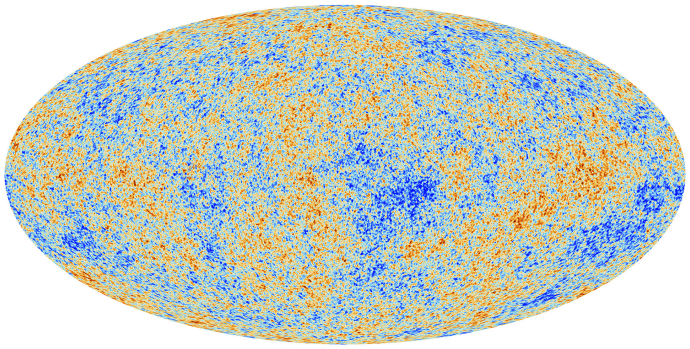

Figure 2.3: *Anisotropies in the cosmic microwave background radiation. Temperature ranges from -300 μK (blue) to +300 μK (red). Copyright: ESA and the Planck Collaboration [26].*

The primary anisotropies are of particular interest, as they give us information about cosmological parameters at the time of decoupling. One part of these anisotropies were formed from the competition between the attractive gravity of matter and the repulsive pressure of photons which led to oscillations propagating with the speed of sound, so called baryon acoustic oscillations. This continued until photons decoupled from matter which froze these density oscillations into the CMB. These oscillations change in a Universe containing dark matter, as this extra matter would deepen the gravitational potential well.

By expanding the CMB in spherical harmonics, one obtains a power spectrum which shows the angular scale of the anisotropies. By looking at the features of this spectrum one can get information about cosmological parameters at the time of decoupling.

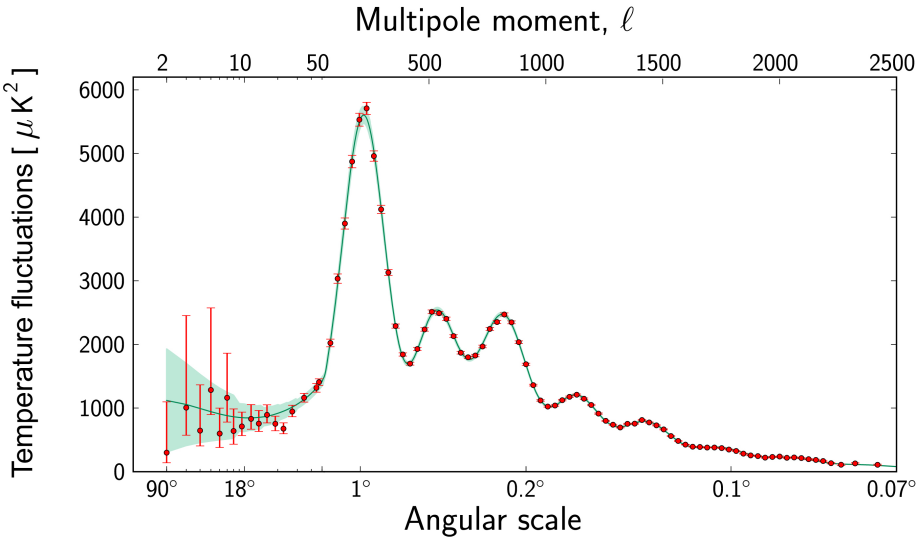

Figure 2.4: *The CMB decomposed into an angular power spectrum. Red dots are measurements done by the Planck telescope, the green curve is a best fit of the ΛCDM model, which is the standard model of cosmology. The pale green area are variations of the standard model that agree with the data. Copyright: ESA and the Planck Collaboration [27].*

As mentioned previously, a homogeneous and isotropic universe on the level of galaxy clusters admits three possibilities for the curvature of the universe arise: flat, open or closed.

Looking at the angular power spectrum fig.(2.4), the first peak is related to the curvature of the universe and observations show that it is flat, $\Omega = 1$ [1]. The second and third peak are related to the matter density and observations give $\Omega_b h^2 = 0.022$ for baryons and $\Omega_{DM} h^2 = 0.12$ for dark matter [1], where h is the reduced Hubble constant $h = \frac{H}{100}$.

The existence of dark matter influences how structures form in the universe. According to the ΛCDM model (Λ for dark energy, CDM stands for cold dark matter, which will be explained later), which is the standard model of cosmology, dark matter decoupled from photons before baryons did. When the baryons decoupled, they fell into the gravitational potential well of the dark matter, where inhomogeneities were amplified and gave rise to the structures we see today. Structures would form later than what we observe in a universe without dark matter.

One important distinction regarding dark matter is whether it is cold (non-relativistic), hot (relativistic) or warm (slightly relativistic). Hot dark matter (HDM) implies that large structures form first, which then fragment into smaller structures. Cold dark matter (CDM), on the other hand form small structures first, which then merge into larger structures. Warm dark matter (WDM) is somewhere in between. From simulations we find that dark matter must be cold in order to explain the structures we see today [28], [29]. Simulations with CDM is not entirely without problems however. Simulations in low-mass galaxies give a dark matter distribu-

tion with a steep increase in density for small radii, which clash with the observed flat central density profiles, this is the cusp/core problem [30]. Another problem is that simulations predicts one order of magnitude more dwarf galaxies than what is observed, the dwarf galaxy problem [31]. Theories exist to try to explain these problems, but are not yet conclusive [32], [33], [34].

2.3 Solving the dark matter problem

In the last section we saw evidence of dark matter on different length scales:

- Solar neighborhood - velocity dispersion of Stars
- galactic scale - rotation curves
- galaxy cluster - virial theorem and weak gravitational lensing
- observable universe - anisotropies in the CMB and simulations of structure formation

The two pieces of evidence in the last category above also show us that the evidence for dark matter exist on different time scales, since they concern events that took place in the early universe. I consider three different ways to interpret dark matter:

1. Our understanding of gravity is incorrect
2. Dark matter consists of non-luminous or faint baryonic matter
3. Dark matter consists of one or more new types of particles

The first option suggests that our theories of gravity breaks down for large objects and that a correct theory of gravity would not give rise to any dark matter. Theories of this type are for example MOdified Newtonian Dynamics (MOND), Tensor-Vector-Scalar gravity (TeVeS), $f(R)$ gravity, entropic gravity [35] [36] [37] [38] . One challenge for these theories is that they need to modifiy gravity on several length scales and time scales simultaneously. Another challenge is to explain a newly discovered galaxy which contain no dark matter [39].

The non-luminous matter of option number two could be Massive Astrophysical Compact Halo Object (MACHOs), which consists of black holes, neutron stars, white dwarfs, faint stars, brown dwarfs and planets. These objects are not very luminous, making them hard to detect, which is why they are missed when summing up all luminous matter. MACHOs can only account for a small fraction of the dark matter, due to big bang nucleosynthesis (BBN) and the angular power spectrum of the CMB. If MACHOs were a large fraction of the dark matter, the abundance of the elements created in the BBN would be higher, since the BBN depend on the baryon to photon ratio [40]. In this thesis I will consider the third option.

2.4 Characteristics of dark matter

Before I introduce the particle candidates, we need to know which properties that it needs to fulfill. We know that dark matter does not interact via the electromagnetic

force, otherwise we would have seen it. This means that it has to be electrically neutral (although there is a proposed type of particle that circumvents this criteria, which I will mention shortly). We know that it interacts via gravitation, which I showed previously. That leaves us with the possibility of interaction via the strong and/or weak nuclear force. Dark matter has to be stable on cosmological time scales, otherwise it would have decayed. It needs to be consistent with the observed $\Omega_{DM}h^2 = 0.12$.

2.5 Production mechanism

Thermal production is the relevant production mechanism for this thesis, but I will briefly cover some alternative mechanisms.

2.5.1 Thermal production

Dark matter is assumed to have been in thermal equilibrium with matter in the early universe by interactions with standard model particles. Annihilations of dark matter particles χ into standard model particles X or vice versa was equally likely i.e. we had the reaction $\chi\chi \leftrightarrow XX$. As the Universe expanded and cooled, Standard Model particles did not have enough energy to produce dark matter particles. As the Universe continued to expand, the density of dark matter was thinned out, such that the probability of two dark matter particles meeting and annihilating became lower. When the temperature became sufficiently low, interactions that changed the number of dark matter particles were negligible, we say that the interactions *freeze out*. This occured when the temperature $T << m_\chi$, where m_χ is the dark matter mass. The effect is that the number of dark matter particles remain constant, which we call the *relic density*. The number density of dark matter can be calculated from the Boltzmann equation

$$\frac{dn_\chi}{dt} + 3Hn_\chi = -\langle\sigma v\rangle(n_\chi^2 - n_{\chi,\mathrm{eq}}^2),$$

where $\langle\sigma v\rangle$ is the thermally averaged self-annihilation cross section. Solving the Boltzmann equation to get the correct relic density today, we require dark matter to have a thermally averaged self-annihilation cross section of [41]

$$\langle\sigma v\rangle = 3 \cdot 10^{-26}\frac{cm^3}{s}.$$

This is consistent with a particle at the weak scale, the so called "WIMP miracle" (Weakly Interacting Massive Particle), as supersymmetry predicts a particle with just these properties.

2.5.2 Non-thermal production

There are several production mechanisms that do not rely on dark matter being in thermal equilibrium with matter in the universe. One of these mechanisms concern

a particle called axion. These axions can form at a phase transition in the early universe. Either in the QCD phase transition, the transition where free quarks are bound into hadrons, or in the Peccei-Quinn phase transition. I will cover these transitions in the discussion of axions. Other production mechanisms are decay of some heavier particle and particle-antiparticle asymmetry. Yet other mechanisms are that dark matter is produced from the decaying inflaton field at the end of inflation, or through a freeze in effect.

2.6 Dark matter particle candidates

There is no shortage of proposed candidates for dark matter. I will only cover a few in them in detail. References are provided for the interested reader.

2.6.1 WIMP

WIMP is perhaps the most famous category of the dark matter candidates. This type of particle only interacts with baryonic matter via the weak force. WIMPS are CDM and are thermally produced in the early universe. I will discuss two contenders for WIMPs, which stem from different fields of physics: SUperSYmmetry (SUSY) and Kaluza-Klein theory, of which the SUSY candidate is the one that has been studied the most.

SUSY is a theory that goes beyond the standard model of particle physics and gives every bosonic field a corresponding fermionic partner and every fermionic field a corresponding bosonic partner. One of the motiviations behind SUSY comes from the Higgs boson, which have a smaller mass than expected. SUSY tries to solve this by reducing the effect of loop diagrams due to cancellations from superpartner loop diagrams and therefore gives the Higgs boson a smaller mass. The lightest stable WIMP candidate from SUSY is the lightest of the four neutralinos. These particles are neutral combinations of bino, wino and the higgsinos, which are superpartners of the B, W and Higgs bosons. The mass scale of the lightest neutralino is around 10 GeV - 10 TeV [42].

Kaluza-Klein theory is a classical field theory which unifies gravitation and electromagnetism in a five dimensional spacetime. This theory provides a photon and a neutrino as WIMP candidates, both with masses in the TeV range [43].

2.6.2 Axions

Axions arise as a result of explaining the lack of observed CP conservation of the strong nuclear force. This particle is abundantely created during the Big Bang, either through the QCD phase transition or the so called Peccei-Quinn phase transition, and it was never in thermal equilibrium with Standard Model particles. It is CDM, even with its small mass of $\sim 10^{-6} - 1$ eV, because of interactions with instantons [44].

2.6.3 Sterile neutrinos

A type of neutrino that doesn't interact electro-weakly, although they mix with the active neutrinos. This candidate is WDM and have a mass range in keV's [45].

2.6.4 Other candidates

FIMPs: Feebly Interacting Massive Particles. These particles interacted so weakly with Standard Model particles, that they never reached thermal equilibrium. These particles were produced from Standard Model particles through decay or annihilations, until the temperature became too cold, the freeze-in effect [46]. WIMPzillas: superheavy WIMP with masses of 10^{10} GeV. Not in thermal equilibrium in the early universe
SIMPs: Strongly Interacting Massive Particles. These particles interact so strongly that they will never be able to reach a detector.
WISPs: Weakly Interacting Slim Particles: particles of sub-eV mass.
CHAMPs: CHArged Massive Particles: These particles actually have a non-zero electric charge, but they are massive enough to have avoided detection via electromagnetism.
Hidden-sector DM: a type of dark matter which does not react much with standard model particles
Other proposed particles are for instance Cryptons,Q-balls, Little Higgs, Light scalar DM.

2.7 Experiments

There are basically three different types of experiment one can use to detect dark matter: direct detection, indirect detection and collider experiments. Direct detection experiment searches for dark matter that interacts with a baryonic nuclei through looking at the recoil of the nuclei. Indirect detection tries to detect the annihilation products of self-annihilating dark matter. Dark matter could potentially be created in collider experiments by smashing baryonic particles together. I will focus mostly on the indirect detection experiments, as this is relevant to this thesis.

2.7.1 Indirect detection

I divide indirect detection into three main channels: gamma-ray photons (γ), cosmic rays (CR) and neutrinos (ν). The way indirect detection works is searching for a flux of annihilation products of dark matter which can not be explained by other astrophysical processes. This flux can occur either at a line frequency or be spread out over many frequencies. For a line frequency, one has to be sure that no astrophysical processes can mimic the signal. For a flux that is spread out, it is important to have a model of the background. This section is based on Cirelli, which also contains references for the different experiments [47].

2.7.1.1 Gamma rays

For γ we are interested in the reaction $\chi\bar{\chi} \to X \to \gamma\gamma$, where χ ($\bar{\chi}$) is dark matter (anti dark matter) and X is a pair of any of the following standard model particles $e^+e^-, \mu^+e^-, \tau^+\tau^-, b\bar{b}, t\bar{t}, W^+W^-$. One advantage of looking at gamma rays is that they can be traced back to their source. The main drawback is that there is a large background of gamma rays.

Earth's atmosphere is opaque to gamma radiation. We can solve this in two ways: observe from space or observe induced particles showers from the ground. In the first category we have Fermi LAT which observe gamma ray energies of about ~ 20 MeV - 300 GeV. GAMMA-400 is a planned experiment to be launched in 2019. It has a similar energy range as Fermi LAT, but a higher angular resolution and energy resolution.

On the ground we use different type of Cherenkov telescopes, which detect Cherenkov light by particles produced in the atmosphere by gamma rays, but also by cosmic rays. The most common type of Cherenkov telescopes in this context are Imaging Atmospheric Cherenkov Telescopes (IACTs) and they are commonly sensitive to gamma ray energies of 10 GeV - 100 TeV. One drawback is that they can't distinguish the sign of particles. Notable IACTs are HESS, MAGIC, VERITAS and in the future CTA, which will provide a higher sensitivity. The HAWC observatory is a water-based Cherenkov telescope located at a high altitude. It is sensitive to gamma energies of > 100 GeV, which means it is sensitive to a high mass dark matter particle.

2.7.1.2 Cosmic rays

Cosmic rays are primarily comprised of pp^- and e^-e^+ and we consider $\chi\bar{\chi} \to X \to pp^+$,$e^-e^+$, where X is some quark and gauge boson state in the case of pp^- and a leptonic state in the case of e^-e^+.

The advantage and disadvantage of this technique is opposite to that of gamma rays: there is a low background when looking at the anti-matter component, it is not possible to trace the cosmic rays back to their source. In space we have PAMELA and AMS, both of which have a magnetic spectrometer which measures sign and charge of particles. PAMELA is sensitive to energies of 100 MeV - 100 GeV and AMS is sensitive to 100 MeV - TeV. GAPS is a planned space-based experiment which will be able to detect anti-deuterons.

ATIC is a balloon-borne experiment which is sensitive to 100 GeV - 100 TeV. The drawback of this experiment is that it cannot distinguish matter from anti-matter.

On the ground we have Auger, which is an Ultra High Energy Cosmic Ray (UHECR) detector, sensitive to $> 10^{19}$ eV, which means it could potentially find superheavy dark matter, $> 10^{12}$ GeV.

2.7.1.3 Neutrinos

The relevant reactions are $\chi\bar{\chi} \to X \to \nu$, where X can be W^+W^-,$\mu^+\mu^-$,$\tau^+\tau^-$,$b\bar{b}$,$t\bar{t}$,e^+e^-. One advantage of neutrinos is that they can be traced back to the source. The main drawback is that events are rare, since neutrinos do not interact much.

Water or ice Cherenkov telescopes are used to detect Cherenkov radiation from leptons that are produced by the interaction of neutrinos and the water/ice. IceCube is an ice Cherenkov telescope located at the South Pole and it has an energy threshold of about 100 GeV. IceCube includes DeepCore, which have an energy threshold of about 10 GeV. PINGU is a planned upgrade which will lower the energy threshold to about 1 GeV. IceCube shall be discussed in more detail later, as it is the detector used in this thesis.

Telescopes of the water variety are ANTARES in the mediterranean, which have an energy threshold of about 20 GeV. KM3NeT is a planned extension of ANTARES, consisting of ORCA and ARCA. Super-Kamiokande is a telescope in Japan, with a threshold of about 5 MeV. Hyper-Kamiokande is a planned upgrade.

2.7.2 Direct detection

In direct detection experiments, one measures the recoil energy from a dark matter particle interacting with a baryonic particle. The detectors are of various types: noble gas, scintillator crystal, germanium, cryogenic bolometer, superheated fluid, directional. I base this section on Undagoitia and Rauch, and Baudis [48], [49]. I recommend the interested reader to look within those papers to find references to the individual experiments.

Noble gas detectors typically use xenon or argon and the principle of this type of detector is detecting electrons or photons caused by the recoil energy of an dark matter scattering event. Experiments utilizing this type of detectors are XENON, LUX and ZEPLIN.

Scintillator crystals emits light when excited and are typically made of NaI or CsI crystals. This technique is used by DAMA and KIM.

Germanium detectors generate electron-hole pairs during an event, which are carried to electrodes by an electric field where they are detected. This method is sensitive to dark matter of a few GeV in mass. CoGeNT is an example of this detector.

Cryogenic bolometers detects phonons, which are vibrations of the crystal lattice. SuperCDMS and EDELWEISS uses this detector.

Superheated fluid detectors uses fluid that is kept in a temperature above its boiling point. A deposit of recoil energy creates bubbles. By studying the size of these bubbles gives information about the amount of energy deposited. Examples of experiments using this method are COUPP, PICO and SIMPLE.

Directional detectors looks at the direction of recoils and compare with the expected directional dependence of dark matter. DRIFT is an example of such a detector.

2.7.3 Collider experiments

Dark matter can not be directly detected in dark matter experiments, since they don't interact with the detectors. Dark matter could be indirectly inferred however, by smashing together baryons and summing up the momentum of all resulting particles. If some momentum is missing, it could mean that some momentum was carried

away by a dark matter particle. One strength of these searches are that they can be analyzed in a model independent approach using an effective field theory [50]. Colliders are especially suited for dark matter in the < 10 GeV or if the interactions are governed by a spin-dependent operator [50].

2.8 Effective field theory

An effective field theory (EFT) is an approximation of some larger theory, valid at some subset of the parameters. For instance an EFT could be valid in a low energy regime, with high energy behavior being corrections. Fermi's theory of beta decay is an example of an EFT of electroweak interactions and general relativity is perhaps an EFT of quantum gravity.

The starting point for constructing an EFT is choosing the relevant energy scale E, which is small compared to the energy scale Λ of the full theory (which doesn't need to be known), and writing down the Lagrangian:

$$\mathcal{L} = \sum_i c_i \hat{\mathcal{O}}_i, \tag{2.10}$$

where c is the so-called Wilson coefficient and $\mathcal{O}$ is an operator. The sum contain infinite terms, but if the condition $E/\Lambda << 1$ is fulfilled, higher order operators will be suppressed by higher powers of E/Λ, which admits a perturbative approach.

The energy scale of interest to us is the square of momentum transfer q between a dark matter particle elastically scattering of a nuclei. This transfer is on the order of $\sim$ keV. If we assume that the interaction between a dark matter particle and a nuclei is mediated by some (unknown) gauge boson of mass around the weak scale $m_W = 246$ GeV, we see that our condition $E/\Lambda << 1$ is fulfilled.

As we have seen, cold, i.e. non-relativistic, dark matter is favoured from the observation of structure formation in the Universe, we thus want to construct a non-relativistic EFT (NREFT). In order to find the operators of the theory, we need to consider the scattering kinematics and which symmetries we have. The momentum transfer $\vec{q}$ is given by $\vec{q} = \vec{p}' - \vec{q} = \vec{k}' - \vec{k}$, where $\vec{p}'$ ($\vec{k}'$) is the momentum of the WIMP (nuclei) after scattering and $\vec{p}$ ($\vec{k}$) is the momentum of the WIMP (nuclei) before scattering. We require a NREFT to be Galilean invariant. The kinematic invariants available are the momentum transfer $\vec{q}$ and the relative velocity between the WIMP and nuclei $\vec{v} = \vec{v}_{\chi,in} - \vec{v}_{N,in}$. This velocity operator is not Hermitian, instead we define the Hermitian transverse velocity $\vec{v}^{\perp} \equiv \vec{v} + \frac{\vec{q}}{2\mu}$, where μ is the reduced mass in the WIMP-nucleon system. Note that $\vec{v}^{\perp} \cdot \vec{q} = 0$ [51]. Other than the kinematic invariants, we can use the spin of the WIMP and nuclei and we can also use the unit matrix in the WIMP-nucleon system. Our operators needs to be Hermitian, which allows the following building blocks.

$$\mathbb{1}_{\chi N} \quad \hat{\mathbf{S}}_{\chi} \quad \hat{\mathbf{S}}_N \quad \hat{\mathbf{v}}^{\perp} \quad i\frac{\hat{\mathbf{q}}}{2m_N}, \tag{2.11}$$

where the hermiticity of the above operators was proved by Fitzpatrick et. al in [51]. Utilizing these Hermitian, Galilean invariant building blocks gives the following

operators to first order in spin and transverse velocity [52]

$\hat{\mathcal{O}}_1 = \mathbb{1}_{\chi N}$	$\hat{\mathcal{O}}_9 = i\hat{\mathbf{S}}_\chi \cdot \left(\hat{\mathbf{S}}_N \times \frac{\hat{\mathbf{q}}}{m_N}\right)$
$\hat{\mathcal{O}}_3 = i\hat{\mathbf{S}}_N \cdot \left(\frac{\hat{\mathbf{q}}}{m_N} \times \hat{\mathbf{v}}^\perp\right)$	$\hat{\mathcal{O}}_{10} = i\hat{\mathbf{S}}_N \cdot \frac{\hat{\mathbf{q}}}{m_N}$
$\hat{\mathcal{O}}_4 = \hat{\mathbf{S}}_\chi \cdot \hat{\mathbf{S}}_N$	$\hat{\mathcal{O}}_{11} = i\hat{\mathbf{S}}_\chi \cdot \frac{\hat{\mathbf{q}}}{m_N}$
$\hat{\mathcal{O}}_5 = i\hat{\mathbf{S}}_N \cdot \left(\frac{\hat{\mathbf{q}}}{m_N} \times \hat{\mathbf{v}}^\perp\right)$	$\hat{\mathcal{O}}_{12} = \hat{\mathbf{S}}_\chi \cdot \left(\hat{\mathbf{S}}_N \times \hat{\mathbf{v}}^\perp\right)$
$\hat{\mathcal{O}}_6 = \left(\hat{\mathbf{S}}_\chi \cdot \frac{\hat{\mathbf{q}}}{m_N}\right)\left(\hat{\mathbf{S}}_N \cdot \frac{\hat{\mathbf{q}}}{m_N}\right)$	$\hat{\mathcal{O}}_{13} = i\left(\hat{\mathbf{S}}_\chi \cdot \hat{\mathbf{v}}^\perp\right)\left(\hat{\mathbf{S}}_N \cdot \frac{\hat{\mathbf{q}}}{m_N}\right)$
$\hat{\mathcal{O}}_7 = \hat{\mathbf{S}}_N \cdot \hat{\mathbf{v}}^\perp$	$\hat{\mathcal{O}}_{14} = i\left(\hat{\mathbf{S}}_\chi \cdot \frac{\hat{\mathbf{q}}}{m_N}\right)\left(\hat{\mathbf{S}}_N \cdot \hat{\mathbf{v}}^\perp\right)$
$\hat{\mathcal{O}}_8 = \hat{\mathbf{S}}_\chi \cdot \hat{\mathbf{v}}^\perp$	$\hat{\mathcal{O}}_{15} = -\left(\hat{\mathbf{S}}_\chi \cdot \frac{\hat{\mathbf{q}}}{m_N}\right)\left[\left(\hat{\mathbf{S}}_N \times \hat{\mathbf{v}}^\perp\right) \cdot \frac{\hat{\mathbf{q}}}{m_N}\right]$

Table 2.1: Leading order operators in a non-relativistic effective field theory for interactions between a WIMP and a nuclei [52].

I follow the same naming convention as Jiji et. al, with operator $\hat{\mathcal{O}}_2$ excluded as it is second order in transverse velocity [52].

2.9 The detectors of IceCube

The cubic-kilometer neutrino telescope IceCube is located between 1450m and 2450m underground at the South Pole. This telescope consists of two different detectors, one of them is simply called IceCube and it has a neutrino energy threshold of about 100 GeV. The second one, DeepCore, is located inside IceCube and it has lowered the energy threshold to about 10 GeV, allowing it to probe lower WIMP masses. A third detector, AMANDA, was a precursor to the IceCube and DeepCore detectors and it is not in use today. There is a detector located on the surface as well, IceTop surface detector. This detector consists of 162 detector tanks and is used to measure air showers of energies above 100 TeV [53].

PINGU will be placed inside DeepCore and it will lower the energy threshold to about 1 GeV, allowing the hunt for even lower mass WIMPs. The setup of the different detectors can be seen in fig.(2.5).

Neutrinos are detected by Cherenkov radiation from secondary particles, e,μ,τ, produced when the neutrinos interact with the ice. Cherenkov radiation is emitted when the charged particle travels faster than the speed of light in the ice. This radiation is detected by photomultiplier tubes, encased in Digital Optical Modules (DOM). The IceCube detector consist of 78 strings placed in a hexagonal grid with a string spacing of 125m and with 60 DOMs each per string, placed 17m apart. DeepCore consist of 7 additional strings, placed in the center part of the IceCube detector. These strings are deployed between 1860m to 2100m with DOMs placed every 7m with an additional 10 DOMs constituting a veto cap [54]. PINGU will consist of 26 additional strings with 192 DOMs, which will be placed within DeepCore

[53].

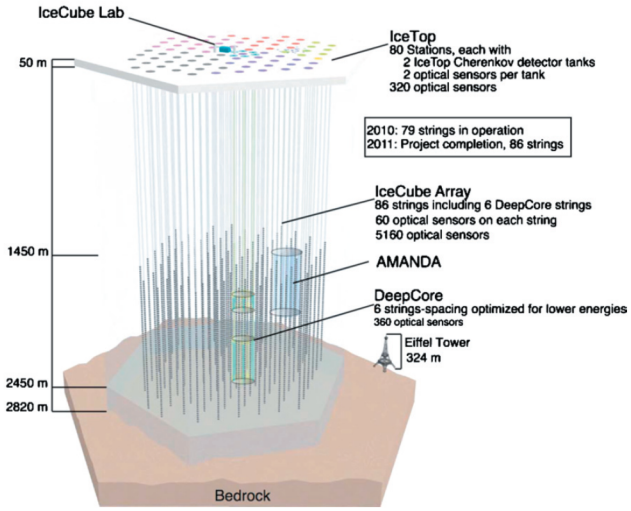

Figure 2.5: *Setup of the IceCube neutrino telescope. The planned PINGU extension will be placed within DeepCore. Figure taken from Wikimedia commons.*

Interactions are divided into charged current (CC), where a $W^{\pm}$ boson is exchanged, or neutral current (NC), where a Z_0 boson is exchanged. For charged currents, the final state is a charged lepton of the same flavor as the initial neutrino. For neutral currents the final state is instead a neutrino with the same flavor as the initial state. We further divide interactions into tracklike and cascadelike events depending on the type of track the neutrino induced particle produce as it propagates. Tracklike events can be used to point back to the neutrino source. Cascadelike events are produced by electromagnetic and hadronic showers and this signature have not been possible to track by IceCube, but PINGU will have have directional reconstruction capability that allows these events in a dark matter search [53]. ν_μ (and $\bar{\nu_\mu}$) produce muons with mostly track-like features, whereas ν_e, ν_τ (and their antiparticles) and neutral current interactions give mostly cascade-like tracks. Muons are more penetrating than the other charged leptons and so they leave the longest tracks in the detector. Since ν_μ give long tracklike features in the detector, they are useful to study dark matter annihilations in the Sun [54]. Other than looking for dark matter, IceCube also researches, among other things, neutrino oscillations and properties of the τ neutrino [53].

3

Method

In this section I will describe the method, assumptions and approximations I use in order to find lower limits on the coupling constants that PINGU will be sensitive to. The starting point is finding the rate at which dark matter particles accumulate in the Sun, followed by the resulting neutrino flux from their annihilation with each other. This flux is used together with experimental input for PINGU, which together with a calculation of background neutrinos can be used to find the sought sensitivity. For the rest of this thesis, I will assume that dark matter only consists of Majorana WIMPs and I will only consider elastic scattering off nuclei.

3.1 WIMP capture by a massive body

This derivation is based on Gould [55]. I will start by deriving the simplest case of WIMP capture by a massive body, which assumes the massive body to be at rest, that it only consist of one type of nucleon and that the WIMP-nucleon cross section is constant.

3.1.1 Simplest case

In order to determine the capture rate of WIMPs by the Sun (or some other massive body), we need to know the inward flux of WIMPs, time spent inside the Sun and the probability to scatter. I will start by laying down the geometry of this problem, continuing with looking at the flux, then looking at the time spent inside the Sun and lastly looking at the probability for scattering.

Consider the Sun as a spherical shell of radius r and thickness dr with a mass which gives rise to a spherically symmetric gravitational field. Consider next another shell placed outside the first shell, with a radius $R >> r$ such that particles at R feel no gravitational field.

Next, we want to know the velocity distribution of dark matter particles, which we here assume are WIMPs. The Sun is assumed to be at rest. Assuming that the particles have an isotropic velocity distribution $f(u)$, where the velocity u is the velocity at infinity with respect to the rest frame of the Sun. The velocity distribution at a surface element of the outer shell can be written

$$\frac{f(u)du}{4\pi} 2\pi \sin\theta = f(u)du\frac{d(\cos\theta)}{2}. \tag{3.1}$$

We wish to know the flux of WIMPs inward, which is simply the expression above times the inward velocity $u = u\cos\theta$

$$f(u)u\cos\theta\frac{d(\cos\theta)}{2}du = -\frac{1}{4}f(u)u\ d(\cos^2\theta)\ du. \tag{3.2}$$

The above expression is valid for angles less than $\pi/2$. Next, we make a change of variables to express the above in angular momentum per mass by

$$J = Ru\sin\theta \implies d(J^2) = d(R^2u^2(1-\cos^2\theta)) = -R^2u^2d(\cos^2\theta). \tag{3.3}$$

The rate N_χ at which the WIMPs enter this region per unit time is then

$$N_\chi = -4\pi R^2\frac{1}{4}f(u)u(-\frac{dJ^2}{R^2u^2})\ du = \pi f(u)\frac{1}{u}d(J^2)du. \tag{3.4}$$

Consider next the velocity of the particles in the shell of the Sun, $w = \sqrt{u^2 + v_{esc}^2}$. The energy per unit mass at infinity is given by

$$\frac{u^2}{2} = \frac{w^2}{2} - \frac{Gm_r}{R}, \tag{3.5}$$

where the last term is $\frac{v_{esc}^2}{2}$, the escape velocity. We want to know how long time the WIMPs spend in the shell, which I call τ. It is given by a differential distance over the inward velocity

$$\tau = \frac{dr}{w\cos\theta}2\Theta(rw - J). \tag{3.6}$$

where the Heaviside function Θ ensures that the particles crosses the Sun and the factor of two ensures it does it twice. From the definition of angular momentum, we can rewrite the above as

$$J = rw\sin\theta = rw\sqrt{1-\cos^2\theta} \implies 1-\cos^2\theta = \frac{J^2}{(rw)^2} \implies \cos\theta = \sqrt{1-\frac{J^2}{(rw)^2}}. \tag{3.7}$$

So we have the time spent in the shell

$$\tau = \frac{dr}{w}\Big(\sqrt{1-\frac{J^2}{(rw)^2}}\Big)^{-1}2\Theta(rw - J). \tag{3.8}$$

Define the rate for a WIMP with velocity w to scatter to a velocity below v_{esc} per unit time $\Omega_v^-(w)$. We can then write the shell capture rate dC as a combination of this rate, time spent in the shell and the rate of incoming particles as

$$dC = \Omega_v^-(w)\cdot\tau\cdot N_\chi = \Omega_v^-(w)\frac{dr}{w}\Big(\sqrt{1-\frac{J^2}{(rw)^2}}\Big)^{-1}2\Theta(rw - J)\pi f(u)\frac{1}{u}d(J^2)du. \tag{3.9}$$

Integrating over the allowed angular momenta gives

$$\begin{aligned}
&2\Omega_v^-(w)\frac{dr}{w}\pi f(u)\frac{1}{u}du\int_0^{r^2w^2}\left(\sqrt{1-\frac{J^2}{(rw)^2}}\right)^{-1}d(J^2)\\
&=[\frac{J^2}{r^2w^2}=s]=2\Omega_v^-(w)\frac{dr}{w}\pi f(u)\frac{1}{u}du\ r^2w^2\int_0^1\left(\sqrt{1-s}\right)^{-1}ds\\
&=2\Omega_v^-(w)dr\ r^2w\pi f(u)\frac{1}{u}du(-2\sqrt{1-s})\Big|_0^1\\
&=4\pi r^2\Omega_v^-(w)dr\ wf(u)\frac{1}{u}du.
\end{aligned}\tag{3.10}$$

We identify the volume element $4\pi r^2$ in the above equation, so the capture rate per shell volume can be written

$$\frac{dC}{dV}=\int_0^\infty\Omega_v^-(w)wf(u)\frac{1}{u}du.\tag{3.11}$$

The fractional WIMP energy loss in a collision is

$$\frac{\Delta E}{E}=\frac{Q}{E}\tag{3.12}$$

The largest value possible for the $Q-$factor is

$$Q=4\frac{M_\chi m}{(M_\chi+m)^2}\cdot\frac{1}{2}M_\chi w^2,\tag{3.13}$$

where the first term is the reduced mass and M_χ is the WIMP mass. The second term is the initial energy, so it cancels with E when we calculate the fractional energy loss. We thus have the constraint

$$\frac{\Delta E_{max}}{E}\leq 4\frac{M_\chi m}{(M_\chi+m)^2}.\tag{3.14}$$

If a particle scatters from velocity w to v_{esc}, the energy loss is

$$\frac{\Delta E_{min}}{E}\geq\frac{w^2-v_{esc}^2}{w^2}=\frac{u^2}{w^2}.\tag{3.15}$$

With these limits, we get the condition for scattering to velocities below v_{esc}

$$\begin{aligned}
(\frac{\Delta E_{max}}{E}-\frac{\Delta E_{min}}{E})\frac{E}{\Delta E_{max}}&=\frac{(M_\chi+m)^2}{4M_\chi m}(\frac{4M_\chi m}{(M_\chi+m)^2}-\frac{u^2}{w^2})\Theta\Big(\frac{4M_\chi m}{(M_\chi+m)^2}-\frac{u^2}{w^2}\Big)\\
&=(1-\frac{u^2}{w^2}\frac{(M_\chi+m)^2}{4M_\chi m})\Theta\Big(1-\frac{u^2}{w^2}\frac{(M_\chi+m)^2}{4M_\chi m}\Big).
\end{aligned}\tag{3.16}$$

The rate of scattering from w to velocities less than v_{esc} is σnw with the above condition, where σ is the WIMP-nucleon cross section and n is the number density of nucleons. If we assume that the cross section is constant, we get

$$\Omega_v^-(w) = \sigma n w(1 - \frac{u^2}{w^2}\frac{(M_\chi + m)^2}{4M_\chi m})\Theta\Big(1 - \frac{u^2}{w^2}\frac{(M_\chi + m)^2}{4M_\chi m}\Big). \tag{3.17}$$

We can rewrite this in order to get a factor of w^{-1} outside the integral that will cancel out in the formula for the capture rate. Omitting the Heaviside function, as it will be rewritten in the same way, we can write

$$\begin{aligned}\Omega_v^-(w) &= \sigma n \frac{1}{w}(w^2 - u^2\frac{(M_\chi + m)^2}{4M_\chi m}) \\ &= \Big[w^2 = u^2 + v_{esc}^2\Big] = \sigma n \frac{1}{w}(v_{esc}^2 + u^2(1 - \frac{(M_\chi + m)^2}{4M_\chi m})) \\ &= \sigma n \frac{1}{w}(v_{esc}^2 - u^2\frac{(M_\chi - m)^2}{4M_\chi m}).\end{aligned} \tag{3.18}$$

So we have

$$\Omega_v^-(w) = \frac{\sigma n}{w}(v_{esc}^2 - u^2\frac{(M_\chi - m)^2}{4M_\chi m})\Theta\Big(v_{esc}^2 - u^2\frac{(M_\chi - m)^2}{4M_\chi m}\Big). \tag{3.19}$$

Assuming that the WIMPs have a Maxwell-Boltzmann distribution

$$f(u)du = n_\chi \frac{4}{\sqrt{\pi}} x^2 e^{-x^2} dx, \tag{3.20}$$

where $x^2 \equiv \dfrac{M_\chi}{2kT_\chi}u^2$, T_χ is the temperature of the WIMP particles, $n_\chi = \frac{\rho_\chi}{M_\chi}$ is the number density of dark matter and k is Boltzmann's constant. We can now write the above with the velocity dispersion as defined by Gould $\bar{v}^2 \equiv \dfrac{3kT_\chi}{M_\chi}$ and $A^2 \equiv \dfrac{3}{2}\dfrac{v_{esc}^2}{\bar{v}^2}\dfrac{4M_\chi m}{(M_\chi - m)^2}$.

$$w\Omega_v^-(w) = \frac{\sigma n v_{esc}^2}{A^2}(A^2 - x^2)\Theta(A - x). \tag{3.21}$$

The capture rate can then be written

$$\frac{dC}{dV} = \int_0^\infty \frac{\sigma n v_{esc}^2}{A^2}(A^2 - x^2)\Theta(A - x) f(x)\frac{1}{u}dx. \tag{3.22}$$

We can rewrite this with the relations

$$\begin{aligned}x^2 = \frac{M_\chi}{2kT_\chi}u^2 \implies \frac{1}{u} = \frac{\sqrt{M_\chi}}{x\sqrt{2kT_\chi}}, \bar{v} = \sqrt{\frac{3kT_\chi}{M_\chi}} \implies \sqrt{M_\chi} = \frac{\sqrt{3kT_\chi}}{\bar{v}} \\ \implies \frac{1}{u} = \frac{\sqrt{3}}{\sqrt{2}x\bar{v}}.\end{aligned} \tag{3.23}$$

So we have

$$\begin{aligned}\frac{dC}{dV} =&\sigma n v_{esc}^2 n_\chi \frac{4}{\sqrt{\pi}}\sqrt{\frac{3}{2}}\frac{1}{\bar{v}}\int_0^A (1-\frac{x^2}{A^2})x^2 e^{-x^2}\frac{1}{x}dx \\ &= \sigma n v_{esc}^2 n_\chi \frac{\sqrt{24}}{\sqrt{\pi}}\frac{1}{\bar{v}}\int_0^A (x-\frac{x^3}{A^2})e^{-x^2}dx \\ &= [\int xe^{-x^2} = -\frac{e^{-x^2}}{2}, \int x^3 e^{-x^2} = -\frac{e^{-x^2}}{2}(1+x^2)] \\ &= \sigma n v_{esc}^2 n_\chi \frac{\sqrt{24}}{\sqrt{\pi}}\frac{1}{\bar{v}}\frac{1}{2}\big[1-e^{-A^2}-\frac{1}{A^2}(1-e^{-A^2}(1+A^2))\big] \\ &= \sigma n v_{esc}^2 n_\chi \frac{\sqrt{6}}{\sqrt{\pi}}\frac{1}{\bar{v}}\big[1-\frac{1-e^{-A^2}}{A^2}\big].\end{aligned} \tag{3.24}$$

The total capture rate is then

$$C = \int_0^R 4\pi r^2 dr \frac{dC}{dV}. \tag{3.25}$$

3.1.2 Several particle species and energy-dependent cross section.

Generalizing eq.(3.17) to include several species of particles is rather straightforward: we replace n with a sum over n_i and replace its mass m with m_i. Generalizing to an energy-dependent cross section is more tricky. The cross section should depend on the final energy which depend on w^2, and also on the momentum transfer Q^2. Let us first construct a **prototype**

$$\Omega_v^-(w,\sigma(w^2,Q^2)) = \sum_i n_i w(1-\frac{u^2}{w^2}\frac{(M_\chi+m_i)^2}{4M_\chi m_i})\Theta\big(1-\frac{u^2}{w^2}\frac{(M_\chi+m_i)^2}{4M_\chi m_i}\big)\int d\sigma_i(w^2,Q^2). \tag{3.26}$$

Instead of integrating over $d\sigma_i$, we integrate over energy by, $d\sigma_i = dE\frac{d\sigma_i}{dE}$. The term outside the integral in our prototype is the fractional energy loss in terms of the maximum fractional energy loss, i.e. it depends on the energy. So we have to move it inside the integral. The energy limits for capture was worked out in the last section, which in our generalization becomes

$$\frac{u^2}{w^2} \leq \frac{\Delta E}{E} \leq \frac{4M_\chi m_i}{(M_\chi+m_i)^2} \implies E\frac{u^2}{w^2} \leq \Delta E \leq E\frac{4M_\chi m_i}{(M_\chi+m_i)^2}. \tag{3.27}$$

These limits on ΔE results in the particle scattering to a velocity less than the escape velocity. Using these limits as the bounds of our integral, we automatically get the right conditions, so we just remove the factor outside the integral. Our new scattering rate is then now given by

$$\Omega_v^-(w,\sigma(w^2,Q^2)) = \sum_i n_i w\ \Theta\Big(1-\frac{u^2}{w^2}\frac{(M_\chi+m_i)^2}{4M_\chi m_i}\Big)\int_{E\frac{u^2}{w^2}}^{E\frac{4M_\chi m_i}{(M_\chi+m_i)^2}} dE\frac{d\sigma_i(w^2,Q^2)}{dE}$$
$$= \sum_i n_i w\ \Theta\Big(1-\frac{u^2}{w^2}\frac{(M_\chi+m_i)^2}{4M_\chi m_i}\Big)\int_{\frac{M_\chi u^2}{2}}^{\frac{2M_\chi^2 m_i w^2}{(M_\chi+m_i)^2}} dE\frac{d\sigma_i(w^2,Q^2)}{dE}. \tag{3.28}$$

3.1.3 Moving body

For a massive body which is not at rest, the velocity distribution of WIMPs has to be modified. In spherical coordinates

$$f(u)du = n_\chi\frac{4}{\sqrt{\pi}}x^2e^{-x^2}dx = n_\chi\frac{4}{\sqrt{\pi}}\int x^2e^{-x^2}dx\frac{d(\cos\theta)d\phi}{4\pi}. \tag{3.29}$$

Changing variables

$$x^2 \to +x_x^2+x_y^2+(x_z+\eta)^2 = x^2+2x\eta\cos\theta+\eta^2, \tag{3.30}$$

where $\eta^2 \equiv \frac{3}{2}(\frac{v_\odot}{\bar{v}})^2$ and $v_\odot$ is the velocity of the Sun in the rest frame of the dark halo. When shifting reference frame the Jacobian x^2dx is not affected and so we get

$$\begin{aligned} f(u)du &\to n_\chi\frac{4}{\sqrt{\pi}}\int x^2e^{-x^2}e^{-\eta^2}e^{-2\eta x\cos\theta}dx\frac{d(\cos\theta)d\phi}{4\pi} \\ &= n_\chi\frac{4}{\sqrt{\pi}}x^2e^{-x^2}e^{-\eta^2}dx\frac{1}{2}\Big[-\frac{1}{2x\eta}e^{-2x\eta\cos\theta}\Big]_{\cos\theta=-1}^{\cos\theta=1} \\ &= n_\chi\frac{4}{\sqrt{\pi}}x^2e^{-x^2}e^{-\eta^2}dx\frac{e^{2x\eta}-e^{-2x\eta}}{4x\eta} = n_\chi\frac{4}{\sqrt{\pi}}e^{-x^2}x^2e^{-\eta^2}dx\frac{\sinh 2x\eta}{2x\eta}. \end{aligned} \tag{3.31}$$

3.1.4 Including Galactic escape velocity

Taking into account the Galactic escape velocity, the velocity distribution of WIMPs need to be modified by a factor

$$\Big[\mathrm{Erf}(\frac{v_{galesc}}{v_{esc}}) - \frac{2}{\sqrt{\pi}}\frac{v_{galesc}}{v_{esc}}e^{\frac{-v_{galesc}^2}{v_{esc}^2}}\Big]^{-1}, \tag{3.32}$$

see Lewin for a derivation [56]. WIMPs that have speeds larger than $v_{galesc}+v_{obs}$ can never be captured. In addition, the velocity distribution needs to be modified for WIMP velocities over $v_{galesc}-v_{obs}$, where $v_{obs} \equiv \eta v_{esc}$

$$f(u)du = u\frac{3}{2}\frac{1}{\sqrt{\pi}\bar{v}^2\eta}(e^{-\frac{(u-v_{obs})^2}{v_{esc}^2}} - e^{-\frac{(v_{galesc})^2}{v_{esc}^2}}). \tag{3.33}$$

3.1.5 Calculating capture rates

Using eq.(3.11) with the modified velocity distribution in sections 3.1.3 and 3.1.4 together with the scattering rate in eq.(3.28) as input in eq.(3.25) gives us the capture rate of dark matter particles by the Sun used in this work. This formula is computed in a modified version of the DMFORMFACTOR Mathematica package [57] by Catena et al. [58], with the radial dependence of the escape velocity and density in the Sun taken from the DARKSUSY FORTRAN package [59]. The density is tabulated for the 16 most abundant isotopes of the Sun: ^{1}H, ^{3}He, ^{4}He, ^{12}C, ^{14}N, ^{16}O, ^{20}Ne, ^{23}Na, ^{24}Mg, ^{28}Si, ^{32}S, ^{40}Ar, ^{40}Ca, ^{56}Fe and ^{58}Ni, where the last isotope is the mean density from the two isotopes ^{58}Ni and ^{60}Ni. All of these isotopes have been used in this work.

The starting point is calculating the differential cross section $\frac{d\sigma_i}{dE}$ in eq.(3.28), which can be written

$$\frac{d\sigma_i(w^2,Q^2)}{dE} = \frac{m_i}{2\pi w^2}\langle|M|^2\rangle_{spin}, \tag{3.34}$$

where the spin averaged matrix element M consist of WIMP response functions $R(v^{\perp},\frac{Q^2}{m_N^2})$ and nuclear response functions $W(y)$, where y is an exponential suppression factor in terms of the transferred momenta and the harmonic oscillator length of the nucleus [51]. These nuclear response functions are taken from Catena and Schwabe [58].

The WIMP response function depend linearly on the coupling constant, which specifies the strength of the interaction between a dark matter particle and a nucleus for a given operator. This is the Wilson coefficient that i mentioned in sec.(2.8), of this effective field theory. The value of the coupling constant is used as input and specified in terms of the inverse square of the Higgs expectation value $m_v = 246.2$ GeV. Together with this value, either isoscalar or isovector coupling is chosen, depending on if the target is a neutron or proton.

As these response functions depend linearly on the coupling constant, the differential cross section and therefore the capture rate C in eq.(3.25) will depend on the square of the coupling constant c, i.e.

$$C \propto c^2. \tag{3.35}$$

This equation is central in this work, since I am investigating the smallest strength of the coupling constant which can be probed by PINGU.

Capture rates are calculated in this thesis for all 14 operators in the NREFT framework that I discussed in sec.(2.8), both isoscalar and isovector.

3.2 Annihilation rates and neutrino flux

Using the capture rate of dark matter particles, we wish to know the annihilation rate and resulting neutrino flux. We can write the self-annihilation $\Gamma(t)$ of two WIMPs

$$\Gamma(t)_a = \frac{1}{2} C_a N^2(t), \tag{3.36}$$

where $N(t)$ is the total number of trapped WIMPs inside the Sun and C_a is related to the annihilation cross-section σ_a. Through capture and annihilation processes, the number of trapped particles change according to

$$\frac{dN}{dt} = C_c(t) - C_a N^2, \tag{3.37}$$

where C_c is the capture rate. Solving this equation gives [59]

$$\Gamma_a = \frac{C_c}{2} \tanh^2 \frac{t}{\tau}, \tag{3.38}$$

where the equilibrium time scale $\tau = \frac{1}{\sqrt{C_c C_a}}$ is much smaller than the current age of the Sun and so

$$\Gamma_a \approx \frac{C_c}{2}. \tag{3.39}$$

From the annihilation rate, we can compute the differential neutrino flux $\frac{d\Phi_\nu}{dE_\nu}$

$$\frac{d\Phi_\nu}{dE_\nu} = \frac{\Gamma_a}{4\pi D^2} \sum_f B_x^f \frac{dN_\nu^f}{dE_\nu}, \tag{3.40}$$

D is the distance between the detector and the Sun, f is the pair annihilation final states and B_x^f are the branching ratios into these states. $\frac{dN_\nu^f}{dE_\nu}$ are the energy distributions of neutrinos generated by state f. I calculate this differential neutrino flux in DARKSUSY [59]. The final states employed in DARKSUSY are $\tau\bar{\tau}, W\bar{W}$ and $b\bar{b}$.

3.3 Event rates

From eq.(3.40) we can compute the number of neutrino events N_ν in a detector in time t by

$$N_\nu = t \int_{E_{th}}^{m_\chi} \frac{d\Phi_\nu}{dE_\nu} A_\nu(E_\nu) dE_\nu d\Omega, \tag{3.41}$$

where E_{th} is the energy threshold of the detector, m_χ is the dark matter mass, A_ν is the effective area of the detector and $d\Omega$ is the angular cone of the detector. The effective area is specific to a detector and it is defined as the area for which the detector detects a neutrino with 100% efficiency.

3.4 Background

In order to find the smallest coupling constant PINGU will be able to probe, we need a knowledge about the background of events. This background consists of

atmospheric muons and atmospheric neutrinos, created in the atmosphere by cosmic ray interaction in the atmosphere, and solar neutrinos from the fusion process inside the Sun. Solar neutrinos have a different energy range than neutrinos from WIMP annihilation and around 1 event per year is expected in the detectors, so I will not consider this background [54]. The remaining neutrino background consists of prompt flux and conventional flux. The prompt flux is roughly a thousand times smaller than the conventional flux in the WIMP mass range and so I will neglect it [60]. So we are left with the conventional flux, which have been tabulated by Honda et. al [61] for the South Pole. Furthermore I use the version of the data that has been averaged over both the azimuthal angle and the seasonal variation of one year.

The atmospheric muons is by far the most important background, with order 10^6 as many events as atmospheric neutrinos. As mentioned in sec(2.9), charged current interactions caused by muon neutrinos give rise to muons and so when looking for muon neutrinos from dark matter annihilations it is important to reduce the background of atmospheric muons. This can be achieved by using vetoing techniques. The vetoing technique consist in rejecting events which start at the outer strings and also by the IceTop detector, as they are far more likely to be caused by muons rather than muon neutrinos. Thus only events that start within the detectors are considered, as these events are more likely to be caused by muon neutrinos rather than muons. Vetoing techniques are more effective for DeepCore, as this detector is surrounded by the IceCube detector and so atmospheric muons are less likely to reach this detector. PINGU will have an even stronger veto, as this detector will be placed within DeepCore [53]. It is not known exactly how effective the vetoing will be for PINGU, so the atmospheric muons is sometimes simply neglected in analyses [53], [62], [63].

Another way to remove the effect of the atmospheric muons when searching for dark matter annihilations from the Sun is to only analyze data when the Sun is below the horizon, as the muons in the direction of the Sun has to pass through the Earth before reaching the detector. This correspond to a winter type scenario, where the local zenith angle is $\geq 90^\circ$ and this is how dark matter searches have been performed for the IceCube and DeepCore detectors [64], [54]. For PINGU, the vetoing techniques is presumed to be good enough to allow for data taking throughout the whole year. DeepCore actually made it feasible to perform dark matter searches from the Sun during summer also, but with a significantly reduced detector volume, as the outer strings are used for identifying atmospheric muons [54].

Further rejection of the background is achieved at the IceCube detectors by sophisticated reconstruction of the tracks in the detectors, using different filters to distinguish between different types of tracks and selecting events with a certain number of DOM hits [54].

To calculate the rate of background neutrinos, I will use the following

$$N_{bg} = t \int_{E_{th}}^{m_\chi} \frac{d\Phi_\nu^{bg}}{dE_\nu} A_\nu(E_\nu) dE_\nu \Delta\Omega, \tag{3.42}$$

where the quantities are the same as in eq.(3.41), with the difference that the flux is from background neutrinos. I consider events contained in the solid angle range

$\Delta\Omega = 2\pi(1-\cos\psi)$, where the acceptance angle ψ is different for PINGU, DeepCore and IceCube.

In calculating the background in the PINGU detector, I will assume data taking all year, since the vetoing techniques are predicted to be strong, even in a summer type scenario. The position of the Sun varies between approximately 66° and 113° zenith angle during the year and so I will average the flux between these angles [54].

Even though PINGU is predicted to reduce atmospheric muons to insignificant levels, I make a conservative prediction by assuming that the vetoing mechanism is not perfect, but instead as strong as for DeepCore.

3.5 Calculation of significance

In order to find the sensitivity of PINGU, I will calculate the significance

$$S = \sqrt{2\Big((N_s + N_{bg})\log\Big(1 + \frac{N_s}{N_{bg}}\Big) - N_s\Big)} \approx \frac{N_s}{\sqrt{N_{bg}}}, \tag{3.43}$$

with N_s and N_{bg} calculated by eq.(3.41) and eq.(3.42) respectively. The above holds if the background N_{bg} is much larger than the dark matter signal N_s [65]. As the dark matter signal N_s is proportional to the capture rate and therefore the square of the coupling constant, see eq.(3.35), I can find what strength of the coupling constant which PINGU will be sensitive to, for a given significance level. In high energy physics, a rejection of the background only hypothesis with a significance of $S = 5$ is the gold standard, appropriate to constitute a discovery. When trying to reject a signal hypothesis on the other hand, a significance of $S = 1.64$ is common [65].

3.6 Astrophysical and experimental input

I present the astrophysical and experimental input used in this thesis below. Uncertainties in these values shall be discussed in the discussion section.

$v_\odot$	220 km $\cdot$ s^{-1}
v_{galesc}	544 km $\cdot$ s^{-1}
$\bar{v}$	270 km $\cdot$ s^{-1}
ρ_χ	0.4 GeV $\cdot$ cm^{-3}

Table 3.1: Astrophysical variables used in this thesis.

The acceptance angle I use for PINGU is taken from Aartsen et al and the effective area from Clark et. al [53], [66]. This effective area is based on a PINGU configuration of 40 strings with 96 DOMs per string but recently the configuration changed to 26 strings of 192 DOMs each. It is stated by the IceCube collaboration that this new configuration will have comparable sensitivities [53]. For IceCube and DeepCore I use acceptance angles and effective areas from Aartsen et. al [54]. The effective area for all detectors is plotted on the next page.

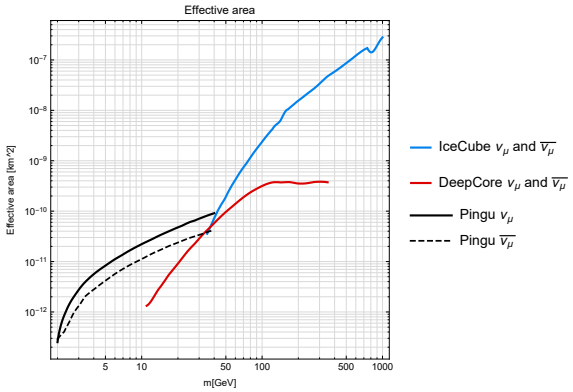

Figure 3.1: *The effective area of the IceCube detectors.*

4

Results

Using eq.(3.43), I have calculated the coupling constant strength that PINGU will be sensitive to with a significance of various sigma levels, for one and three years of data taking. This has been done for 28 operators in the non-relativistic effective field theory framework for a dark matter particle of spin half and I consider dark matter annihilating into either $b\bar{b}$ or $\tau\bar{\tau}$. The analysis is based on PINGU gathering data the whole year and I consider a muon contamination of the same level as in DeepCore. I have found an estimate of this contamination by calculating the neutrino background for DeepCore in a winter type scenario and rescaling this background with observational data, for all background events under an energy of 3000 GeV [54]. This rescaling is expected to be a bit rough, as it assumes the same muon scaling over the whole parameter space.

Dark matter could also annihilate into $W\bar{W}$, which requires a dark matter mass of 80.4 GeV or above. PINGU can not detect neutrinos of energy above 40 GeV and I have found that PINGU will not significantly change the sensitivity to this channel. The region of interest is dark matter particles with low masses and I have chosen to explore the regions between 2 and 100 GeV for the $\tau\bar{\tau}$ channel and between 6 and 100 GeV for the $b\bar{b}$ channel, as annihilations into $b\bar{b}$ is not kinematically accessible at lower masses.

For comparison, I include the coupling constant strength which have been excluded at the 90% confidence level by 3 years of data taking by IceCube and DeepCore, during the wintertime [54]. These exclusion limits are related to the significance S by

$$S = \Phi^{-1}(1 - p), \tag{4.1}$$

where p is the p-value, which is the probability of observing a value at least as extreme as the sample data, assuming the hypothesis of only background to be true. Φ^{-1} is the inverse of the cumulative Gaussian distribution function, called the quantile [67]. Using the above formula, one finds that 90% exclusion limits are equivalent to a significance of 1.28 sigma.

Before presenting the results, I would like to perform a few checks. The dark matter signal depends on the capture rate in eq.(3.25) and as a check of these rates, I have calculated capture rates for a coupling constant strength of $10^{-3}m_v^{-2}$, with m_v defined in sec.(3.1.5), for all 28 operators, with spin half. I include four of these plots on the following page, for operator 1 and operator 4 with both isoscalar and isovector coupling.

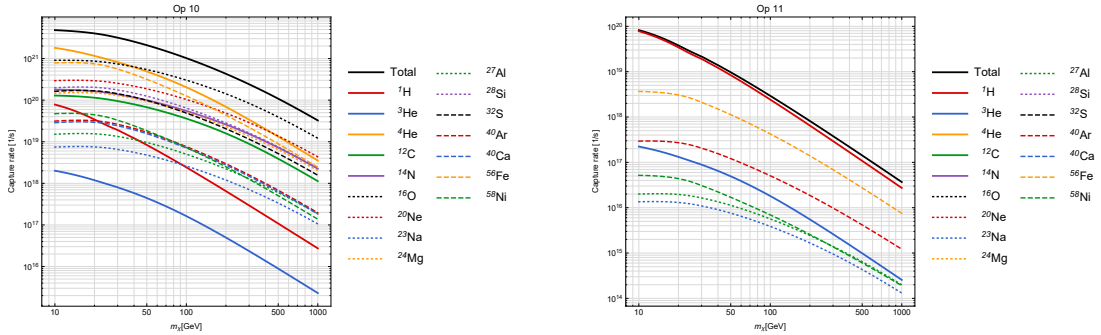

Figure 4.1: Capture rates from operator 1 isoscalar coupling (left) and isovector coupling (right).

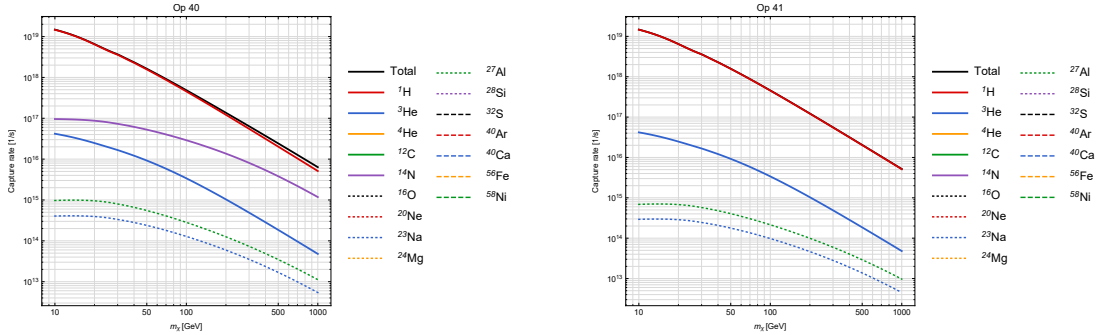

Figure 4.2: Capture rates from operator 4 isoscalar coupling (left) and isovector coupling (right).

These two operators are the most common in literature, as they are fairly simple operators that does not need a full effective field theory framework. They are called the canonical spin independent and spin dependent operator, respectively. The capture rates agree superbly with literature for all 28 operators [58].

Another check is to see if I can reproduce the current 90% IceCube exclusion limits for the DeepCore detector, by using eq.(3.43), where the background consists of atmospheric neutrinos multiplied with a factor to account for muon contamination, as discussed in sec.(3.4) and in the beginning of this chapter. I have performed this check for all 28 operators, for both the $\tau\bar{\tau}$ and $b\bar{b}$ channels. I present the result for operator 1 isocalar, the result is comparable to the other operators.

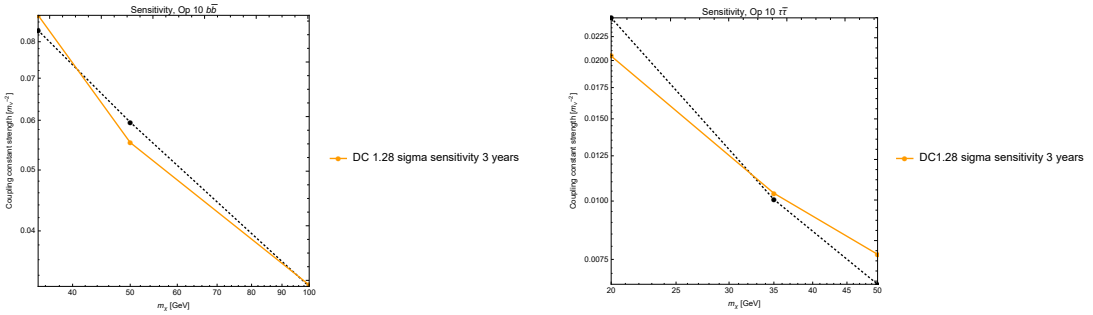

Figure 4.3: Comparison of significance between the DeepCore detector and the present IceCube exclusion limits for operator 1 isoscalar. $b\bar{b}$ channel to the left, $\tau\bar{\tau}$ channel to the right. The fit is reasonably good in the parameter space considered here.

The fit is reasonably good in the dark matter mass range I consider, which validates the way I include muon contaminations to get a conservative upper limit on the background. The error is largest for the $\tau\bar{\tau}$ channel, with the largest relative error in the plot above being 17.2%. For the $b\bar{b}$ channel, the largest relative error is only 7.2% in the plot above. Other operators have comparable relative errors.

Without further ado I now present my sensitivity results for isoscalar coupling. The features of the isovector coupling plots are very similar, so I will not show them here. Instead I have included them in the appendix.

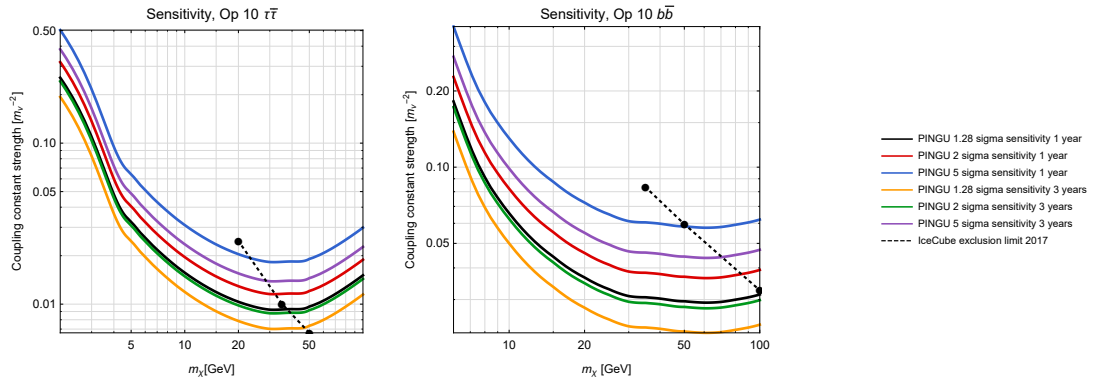

Figure 4.4: Sensitivity studies for operator 1 for the $\tau\bar{\tau}$ channel (left) and $b\bar{b}$ (right).

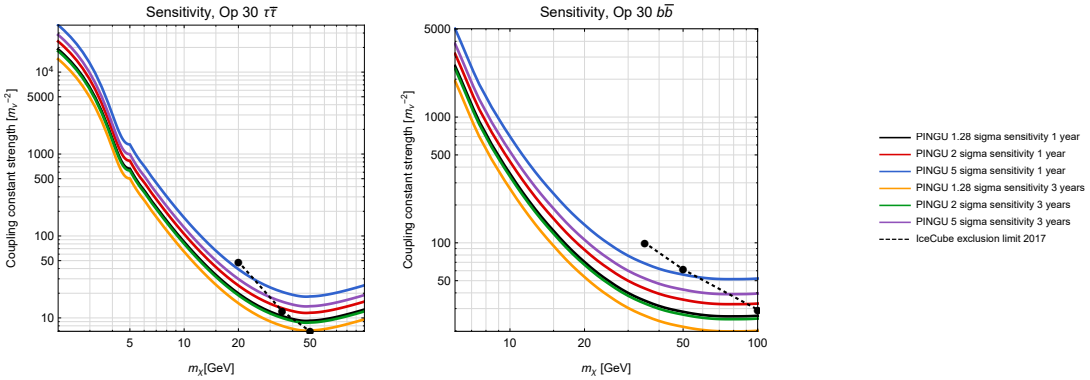

Figure 4.5: Sensitivity studies for operator 3 for the $\tau\bar{\tau}$ channel (left) and $b\bar{b}$ (right).

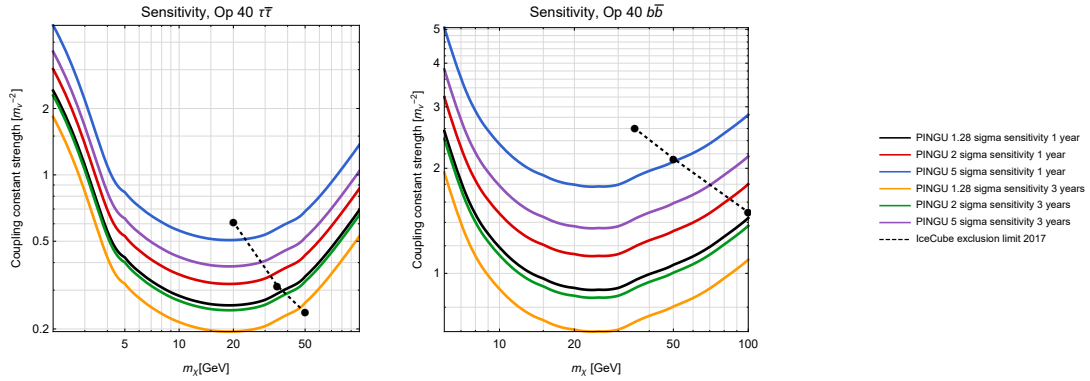

Figure 4.6: Sensitivity studies for operator 4 for the $\tau\bar{\tau}$ channel (left) and $b\bar{b}$ (right).

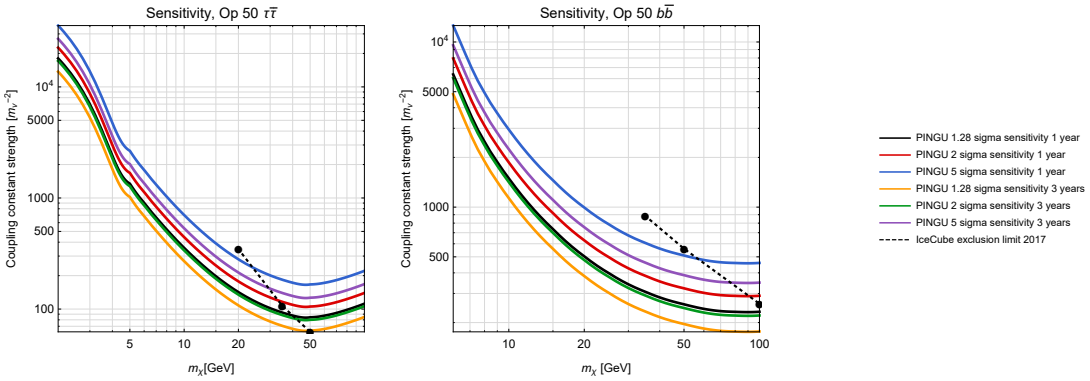

Figure 4.7: Sensitivity studies for operator 5 for the $\tau\bar{\tau}$ channel (left) and $b\bar{b}$ (right).

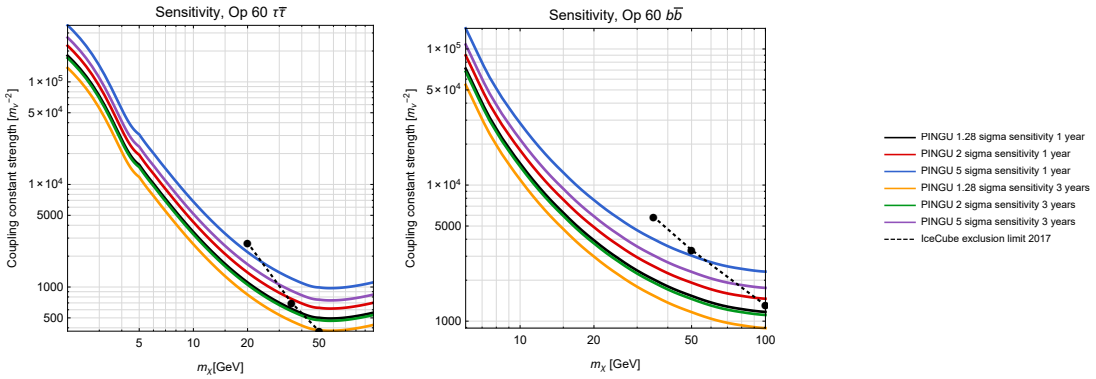

Figure 4.8: Sensitivity studies for operator 6 for the $\tau\bar{\tau}$ channel (left) and $b\bar{b}$ (right).

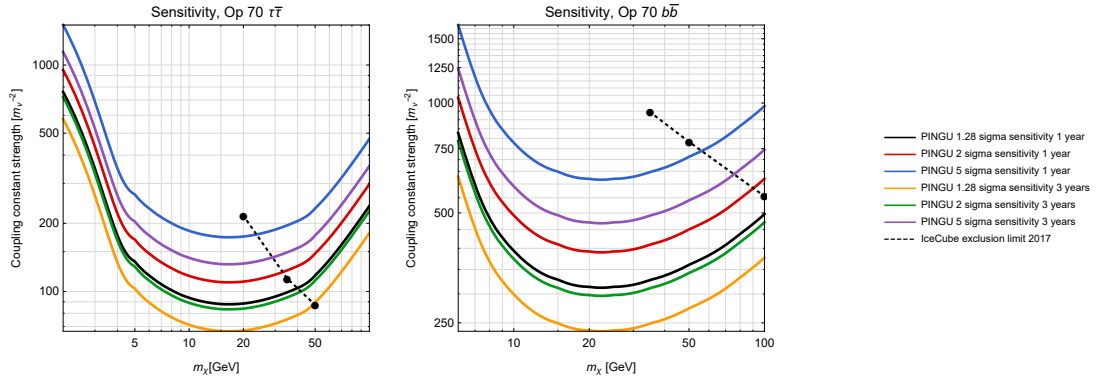

Figure 4.9: Sensitivity studies for operator 7 for the $\tau\bar{\tau}$ channel (left) and $b\bar{b}$ (right).

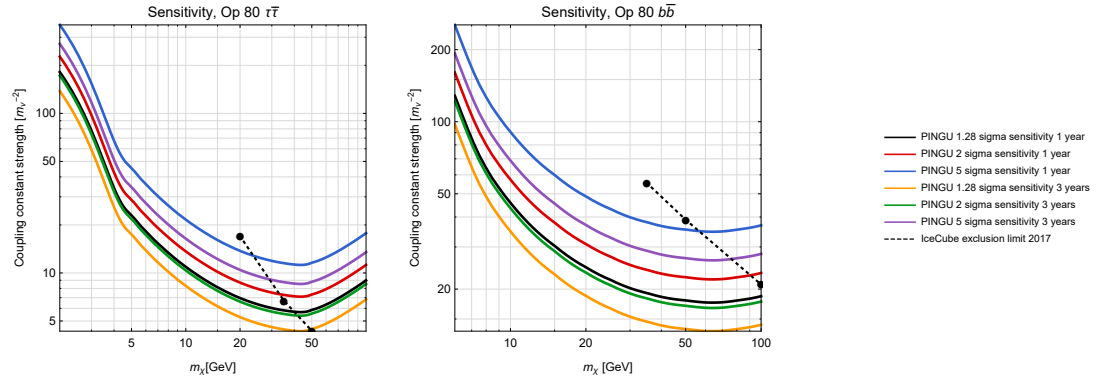

Figure 4.10: Sensitivity studies for operator 8 for the $\tau\bar{\tau}$ channel (left) and $b\bar{b}$ (right).

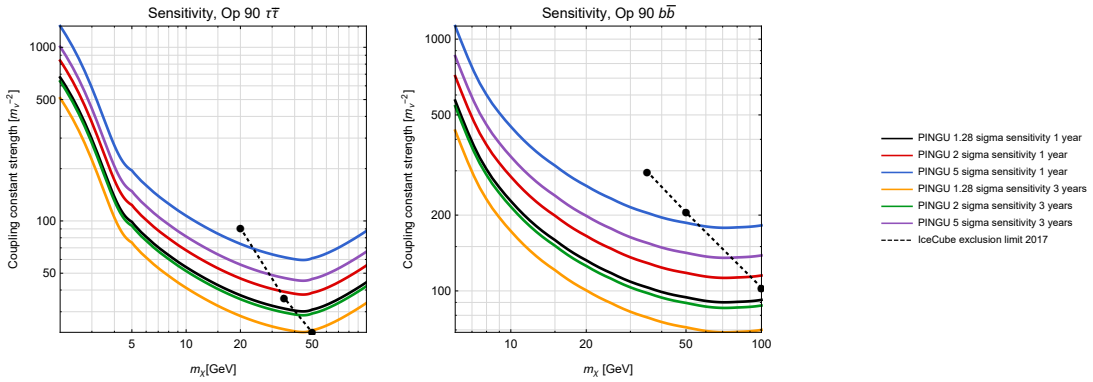

Figure 4.11: Sensitivity studies for operator 9 for the $\tau\bar{\tau}$ channel (left) and $b\bar{b}$ (right).

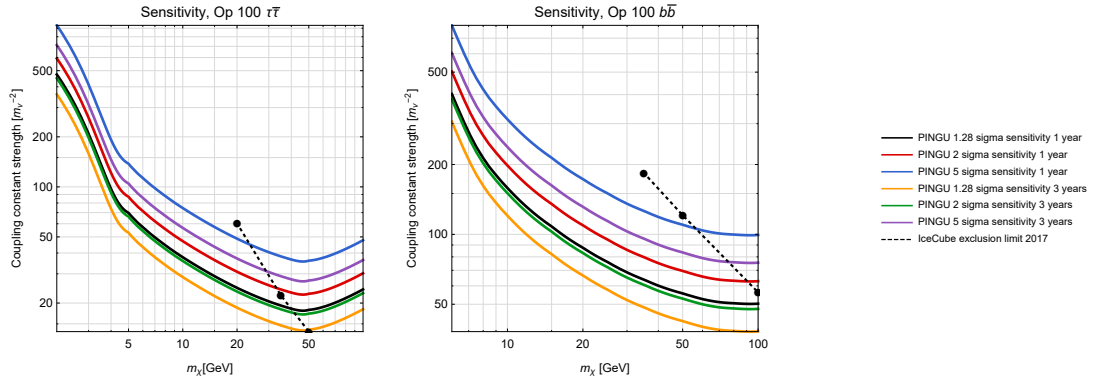

Figure 4.12: Sensitivity studies for operator 10 for the $\tau\bar{\tau}$ channel (left) and $b\bar{b}$ (right).

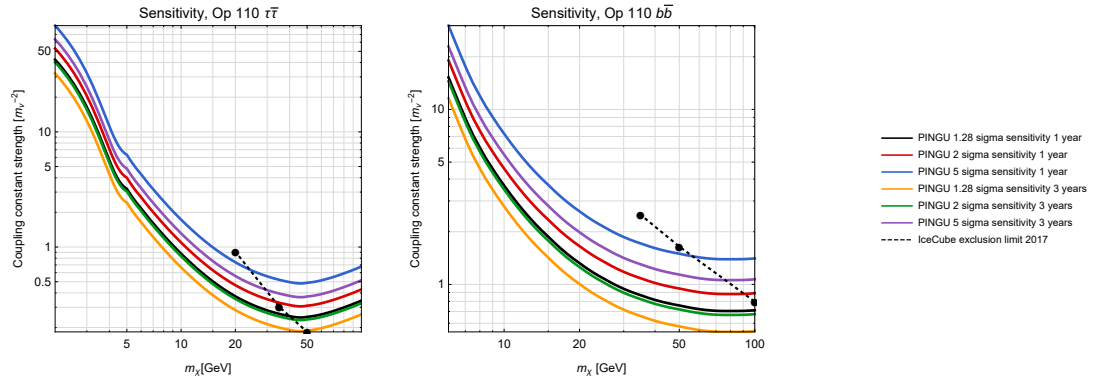

Figure 4.13: Sensitivity studies for operator 11 for the $\tau\bar{\tau}$ channel (left) and $b\bar{b}$ (right).

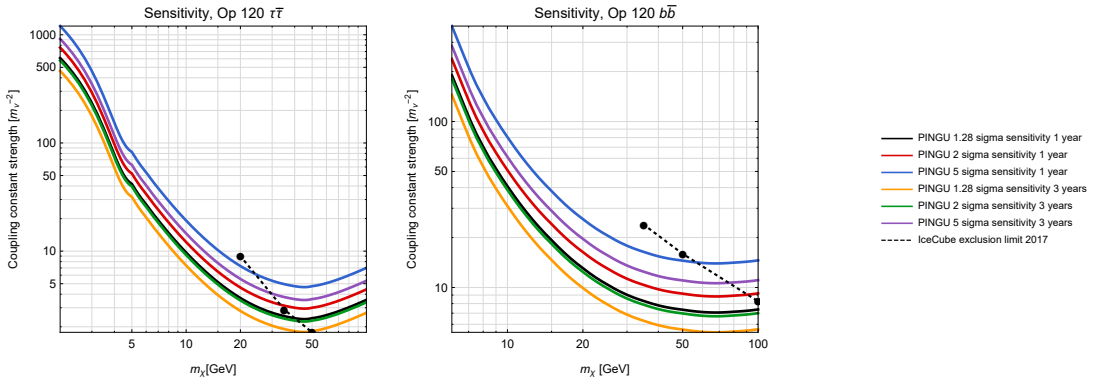

Figure 4.14: Sensitivity studies for operator 12 for the $\tau\bar{\tau}$ channel (left) and $b\bar{b}$ (right).

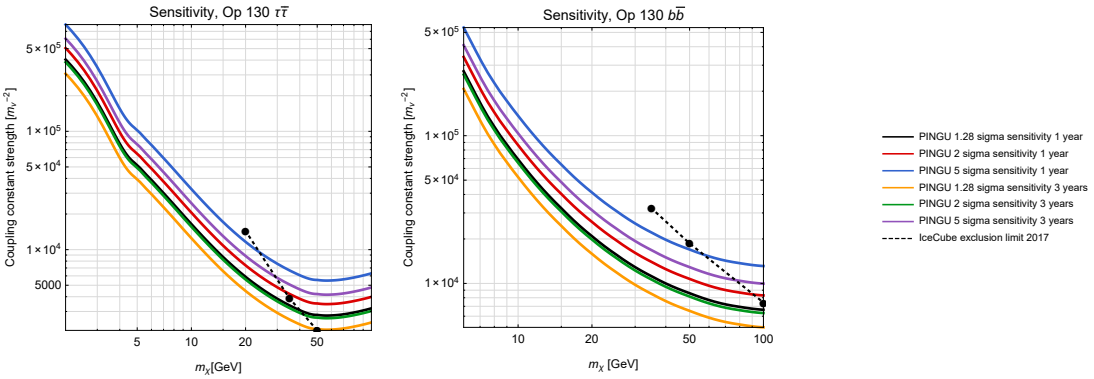

Figure 4.15: Sensitivity studies for operator 13 for the $\tau\bar{\tau}$ channel (left) and $b\bar{b}$ (right).

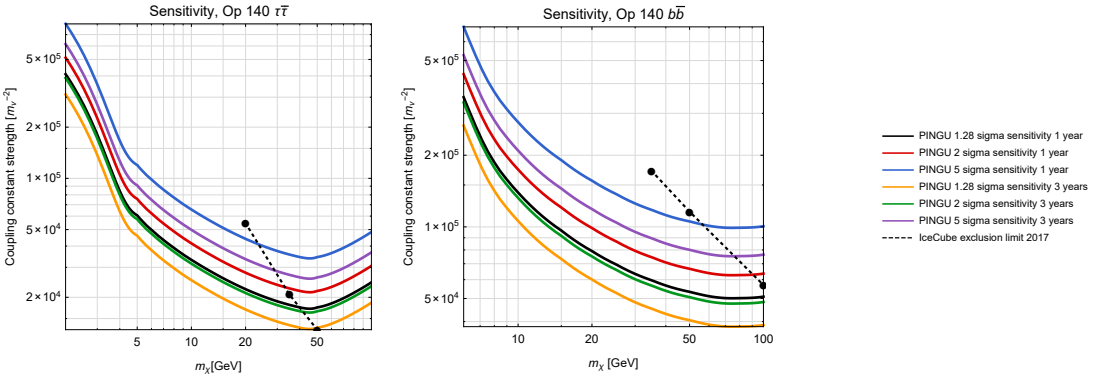

Figure 4.16: Sensitivity studies for operator 14 for the $\tau\bar{\tau}$ channel (left) and $b\bar{b}$ (right).

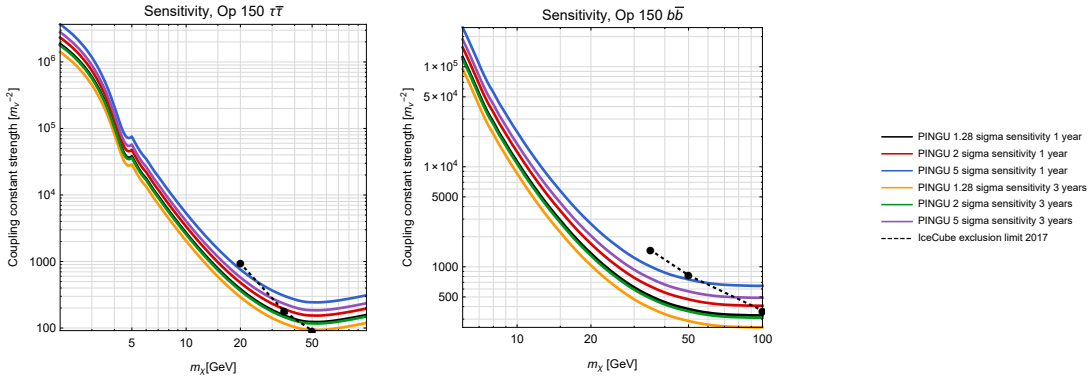

Figure 4.17: Sensitivity studies for operator 15 for the $\tau\bar{\tau}$ channel (left) and $b\bar{b}$ (right).

5

Discussion

From the figures in the previous section, we see that PINGU will improve the current 90% IceCube exclusion limits for a dark matter mass of less than 100 GeV for the $b\bar{b}$ channel and less than $\sim$ 40 GeV for the $\tau\bar{\tau}$ channel after just one year of data taking, for all operators. Extending the data taking to 3 years allows PINGU to extend the upper mass limit to $\sim$ 50 GeV for $\tau\bar{\tau}$. Furthermore PINGU will probe dark matter masses less than 20 GeV for the $\tau\bar{\tau}$ channel and 35 GeV for the $b\bar{b}$ channel, which have been beyond reach for the IceCube and DeepCore detectors so far.

For the $b\bar{b}$ channel, the 90% exclusion limits after 1 year of data taking with PINGU will lower the limits by 65%,55%,11% of present limits for m_χ = 35,50,100 GeV respectively, for all operators. For the $\tau\bar{\tau}$ channel the new limits will be 59%,13% lower than present limits m_χ = 20,35 GeV respectively, for all operators.

5.1 Uncertainties

Uncertainties exist at every step in the calculations and I consider both astrophysical and experimental aspects. All calculations of the dark matter signal hinges on the cross sections calculated in the modified DMFORMFACTOR package. These cross sections can be approximated by a combination of polynomials and exponentials that are different for each operator and each element and as such a detailed quantitative error analysis is highly non-trivial. I will instead give a qualitative analysis, focusing on the largest uncertainties.

5.1.1 Astrophysical

The astrophysical inputs are $v_\odot$, v_{galesc}, $\bar{v}$, ρ_χ, u and n_i as defined in ch.(3). I remind the reader that they are the velocity of the Sun, the galactic escape velocity, the dark matter dispersion, the dark matter density, the dark matter velocity distribution and the number density for a given element, respectively. Of these quantities, the velocities are the most complicated to analyze, since the capture rates have a different dependence on them for all operators and elements. I am assuming that the quantities pertaining to dark matter are the most uncertain of the above, i.e. $\bar{v}$, ρ_χ and u. Of these, it is ρ_χ that is easiest to analyze. The number of dark matter events depends on the dark matter density as $N \propto \rho_\chi$ and the limits on the coupling constant depends on the number of dark matter events as $c \propto \frac{1}{\sqrt{N}}$, therefore $c \propto \frac{1}{\sqrt{\rho_\chi}}$. The uncertainty in the dark matter density is fairly high, with values

reported in the $0.2 - 0.6$ GeV $\cdot$ cm^{-3} range [68]. For $\rho_\chi = 0.4 \pm 0.2$, the relative error in the coupling constant is $\frac{\delta c}{c} = \frac{1}{2} \cdot \frac{\delta \rho_\chi}{\rho_\chi} = 25\%$.

Approximating the dark matter velocity as having an isotropic Maxwell-Boltzmann distribution might be too rough of an assumption. Recent work by Herzog-Arbeitman et al. suggests instead an empirical relation between the dark matter velocity and the velocity of metal-poor stars [69].

5.1.2 Experimental

The statistical uncertainty in the data used to rescale the background to account for muons are roughly $\pm 12\%$ [54]. This gives an uncertainty in the limits of the coupling constant of $\frac{\delta c}{c} = \frac{1}{4} \cdot \frac{\delta N_{bg}}{N_{bg}} = 3\%$, these limits scale with the background as $c \propto N_{bg}^{-1/4}$. If we assume an uncertainty of the same size when calculating signal events in PINGU, we will get an uncertainty in the coupling constant of $\frac{\delta c}{c} = \frac{1}{2} \cdot \frac{\delta N_{bg}}{N_{bg}} = 6\%$, since the coupling constant scale with the signal as $c \propto N^{1/2}$.

5.2 Outlook

It is possible to extend this work in several ways. In particular it is possible to include analyses which increases the dark matter signal and therefore makes the limits stronger. One can for example consider that the trapped WIMPs in the Sun will themselves increase the gravitational attraction and capture more particles, which have been done by Catena and Widmark [70].

One could also look at dark matter that requires multiple scattering events to be captured by the Sun, as have been done by Bramante et. al [71].

Instead of considering only the PINGU detector, sensitivities can be calculated also for IceCube and DeepCore and one can combine this analysis where the effective area of the detectors overlap. It would probably be prudent to do a more thorough analysis of the atmospheric muons in such a analysis.

WIMP searches with neutrino telescopes typically focus on the muon neutrinos, as these leave clear tracks in the detectors. As mentioned in sec.(2.9), PINGU will also have directional reconstruction capability for cascade tracks and so it will be able to find neutrinos of all flavors. This type of analysis would further lower the coupling constant.

The upper dark matter mass considered could be increased from 100 to perhaps 150 or 200 GeV for the $b\bar{b}$ channel, as PINGU will beat the current 90% exclusion limit for a dark matter mass below 100 GeV after just one year of data taking.

One final thing to consider is that my analysis could be applied to other neutrino telescopes, such as Km3Net [72].

6

Conclusion

PINGU is a planned upgrade to the IceCube neutrino telescope and in this thesis I have investigated its prospects for detecting a neutrino flux from dark matter annihilations inside the Sun. More specifically, I have looked at what interaction strength, specified by the coupling constant c, between dark matter and baryonic matter this upgrade will be sensitive to, for dark matter annihilating into either $b\bar{b}$ or $\tau\bar{\tau}$. This analysis have been done in the non-relativistic effective field theory framework for the 28 lowest order operators in spin and transverse velocity for a dark matter particle of spin half and I have compared my results with the 90% exclusion limits, extracted from data taken by the IceCube and DeepCore detector.

I have found that PINGU will improve these limits for a dark matter mass of less than 100 GeV for the $b\bar{b}$ channel and less than ~ 40 GeV for the $\tau\bar{\tau}$ channel, after just one year of data taking, for all 28 operators. The analysis has been performed by looking at muon neutrinos, as these leave a tracklike signature in the detector and can be traced toward the Sun. In the future it would be interesting to also include cascadelike signatures in the analysis, as PINGU will be the first detector of the IceCube observatory with good directional reconstruction capabilities for cascades.

Bibliography

[1] P.A.R Ade, the Planck collaboration, et al. "Planck 2015 results XIII. Cosmological parameters". English. In: *ASTRONOMY & ASTROPHYSICS* 594 (2016;2015;), A13.

[2] Steven Weinberg. *Gravitation and cosmology: principles and applications of the general theory of relativity*. English. New York: Wiley, 1972. ISBN: 9780471925675 ;0471925675;

[3] V. Mukhanov. *Physical Foundations of Cosmology*. Oxford: Cambridge University Press, 2005. ISBN: 0521563984, 9780521563987. URL: http://www-spires.fnal.gov/spires/find/books/www?cl=QB981.M89::2005.

[4] B. Kelvin. *Baltimore lectures on molecular dynamics and the wave theory of light*. https://archive.org/details/baltimorelecture00kelvviala. 1904.

[5] Henri. Poincaré. In: *L' Astronomie* 158 (1906).

[6] Ernst. Öpik. In: *Bull. de la Soc. Astr. de Russie* 21.150 (1915).

[7] J. C. Kapteyn. "First Attempt at a Theory of the Arrangement and Motion of the Sidereal System". In: *Astrophysical journal* 55 (May 1922), p. 302. DOI: 10.1086/142670.

[8] J. H. Oort. "The force exerted by the stellar system in the direction perpendicular to the galactic plane and some related problems". In: *Bulletin of the Astronomical Institutes of the Netherland* 6 (Aug. 1932), p. 249.

[9] F. Zwicky. "Die Rotverschiebung von extragalaktischen Nebeln". German. In: *Helvetica Physica Acta* 6 (1933;), pp. 110–127.

[10] F. Zwicky. "On the Masses of Nebulae and of Clusters of Nebulae". In: *Astrophysical Journal* 86 (Oct. 1937), p. 217. DOI: 10.1086/143864.

[11] S. Smith. "The Mass of the Virgo Cluster". In: *Astrophysical Journal* 83 (Jan. 1936), p. 23. DOI: 10.1086/143697.

[12] E. Holmberg. "On the Clustering Tendencies among the Nebulae." In: *Astrophysical Journal* 92 (Sept. 1940), p. 200. DOI: 10.1086/144212.

[13] Burbidge E.M. and Burbidge G.R. In: *AJ* 10 (1961), p. 66.

[14] G. de Vaucouleurs. "The Apparent Density of Matter in Groups and Clusters of Galaxies." In: *Astrophysical Journal* 131 (May 1960), p. 585. DOI: 10.1086/146871.

[15] Steven Weinberg. *Cosmology*. English. Oxford: Oxford University Press, 2008. ISBN: 0191523607;9780191523601;9780198526827;0198526822;

[16] J. A. Tyson, F. Valdes, and R. A. Wenk. "Detection of systematic gravitational lens galaxy image alignments - Mapping dark matter in galaxy clusters". In:

Astrophysical Journal Letters 349 (Jan. 1990), pp. L1–L4. DOI: 10.1086/185636.

[17] Douglas Clowe et al. "A direct empirical proof of the existence of dark matter". In: *Astrophysical Journal.* 648 (2006), pp. L109–L113. DOI: 10.1086/508162. arXiv: astro-ph/0608407 [astro-ph].

[18] K. C. Freeman. "On the Disks of Spiral and S0 Galaxies". In: *Astrophysical Journal* 160 (June 1970), p. 811. DOI: 10.1086/150474.

[19] D. H. Rogstad and G. S. Shostak. "Gross Properties of Five Scd Galaxies as Determined from 21-CENTIMETER Observations". In: *Astrophysical Journal* 176 (Sept. 1972), p. 315. DOI: 10.1086/151636.

[20] R. N. Whitehurst and M. S. Roberts. "High-Velocity Neutral Hydrogen in the Central Region of the Andromeda Galaxy". In: *Astrophysical Journal* 175 (July 1972), p. 347. DOI: 10.1086/151562.

[21] M. S. Roberts and A. H. Rots. "Comparison of Rotation Curves of Different Galaxy Types". In: *Astronomy and Astrophysics* 26 (Aug. 1973), pp. 483–485.

[22] Salpeter E. E. Krumm N. "Rotation curves, mass distributions and total masses of some spiral galaxies". In: *Astronomy and Astrophysics* 56 (1977), pp. 465–468.

[23] Albert Bosma. "The distribution and kinematics of neutral hydrogen in spiral galaxies of various morphological types". PhD thesis. 1978.

[24] W. K. Jr.; Thonnard N. Rubin V. C.; Ford. "Rotational properties of 21 SC galaxies with a large range of luminosities and radii, from NGC 4605 to UGC 2885". In: *Astrophysical Journal* 238 (6/1980), pp. 471–487.

[25] D. J. Fixsen. "The Temperature of the Cosmic Microwave Background". In: *Astrophysical Journal* 707 (Dec. 2009), pp. 916–920. DOI: 10.1088/0004-637X/707/2/916. arXiv: 0911.1955.

[26] ESA. *Planck CMB.* http://www.esa.int/spaceinimages/Images/2013/03/Planck_CMB, accessed June 11, 2018. 2013. URL: http://www.esa.int/spaceinimages/Images/2013/03/Planck_CMB.

[27] ESA. *Planck power spectrum.* http://www.esa.int/spaceinimages/Images/2013/03/Planck_Power_Spectrum, accessed June 11, 2018. 2013.

[28] Darren Reed et al. "Evolution of the density profiles of dark matter haloes". In: *Monthly Notices of the Royal Astronomical Society* 357.1 (2005), pp. 82–96. DOI: 10.1111/j.1365-2966.2005.08612.x. eprint: /oup/backfile/content_public/journal/mnras/357/1/10.1111/j.1365-2966.2005.08612.x/2/357-1-82.pdf. URL: +http://dx.doi.org/10.1111/j.1365-2966.2005.08612.x.

[29] Toshiyuki Fukushige, Atsushi Kawai, and Junichiro Makino. "Structure of dark matter halos from hierarchical clustering. 3. Shallowing of the Inner cusp". In: *Astrophys. J.* 606 (2004), pp. 625–634. DOI: 10.1086/383192. arXiv: astro-ph/0306203 [astro-ph].

[30] W. J. G. de Blok. "The Core-Cusp Problem". In: *Adv. Astron.* 2010 (2010), p. 789293. DOI: 10.1155/2010/789293. arXiv: 0910.3538 [astro-ph.CO].

[31] Mario Mateo. "DWARF GALAXIES OF THE LOCAL GROUP". In: *Annual Review of Astronomy and Astrophysics* 36.1 (1998), pp. 435–506. DOI: 10.1146/annurev.astro.36.1.435. eprint: https://doi.org/10.1146/

annurev.astro.36.1.435. URL: https://doi.org/10.1146/annurev.astro.36.1.435.

[32] Julio F. Navarro, Vincent R. Eke, and Carlos S. Frenk. "The cores of dwarf galaxy halos". In: *Mon. Not. Roy. Astron. Soc.* 283 (1996), pp. L72–L78. DOI: 10.1093/mnras/283.3.72L,10.1093/mnras/283.3.L72. arXiv: astro-ph/9610187 [astro-ph].

[33] A. Pontzen and F. Governato. "How supernova feedback turns dark matter cusps into cores". In: *Mon. Not. Roy. Astron. Soc.* 421 (Apr. 2012), pp. 3464–3471. DOI: 10.1111/j.1365-2966.2012.20571.x. arXiv: 1106.0499.

[34] Joshua D. Simon and Marla Geha. "The Kinematics of the Ultra-Faint Milky Way Satellites: Solving the Missing Satellite Problem". In: *Astrophys. J.* 670 (2007), pp. 313–331. DOI: 10.1086/521816. arXiv: 0706.0516 [astro-ph].

[35] M. Milgrom. "A modification of the Newtonian dynamics as a possible alternative to the hidden mass hypothesis". In: *Astrophysical Journal* 270 (July 1983), pp. 365–370. DOI: 10.1086/161130.

[36] Jacob D. Bekenstein. "Relativistic gravitation theory for the MOND paradigm". In: *Phys. Rev.* D70 (2004). [Erratum: Phys. Rev.D71,069901(2005)], p. 083509. DOI: 10.1103/PhysRevD.70.083509,10.1103/PhysRevD.71.069901. arXiv: astro-ph/0403694 [astro-ph].

[37] H. A. Buchdahl. "Non-linear Lagrangians and cosmological theory". In: *Monthly Notices of the Royal Astronomical Society* 150 (1970), p. 1. DOI: 10.1093/mnras/150.1.1.

[38] Erik Verlinde. "On the origin of gravity and the laws of Newton". In: *Journal of High Energy Physics* 2011.4 (2011), p. 29. ISSN: 1029-8479. DOI: 10.1007/JHEP04(2011)029. URL: https://doi.org/10.1007/JHEP04(2011)029.

[39] Pieter van Dokkum et al. "A galaxy lacking dark matter". In: (2018).

[40] Richard Cyburt. "Primordial Nucleosynthesis for the New Cosmology: Determining Uncertainties and Examining Concordance". In: 70 (Jan. 2004).

[41] Joakim Edsjo and Paolo Gondolo. "Neutralino relic density including coannihilations". In: *Phys. Rev.* D56 (1997), pp. 1879–1894. DOI: 10.1103/PhysRevD.56.1879. arXiv: hep-ph/9704361 [hep-ph].

[42] Stephen P. Martin. "A Supersymmetry primer". In: (1997). [Adv. Ser. Direct. High Energy Phys.18,1(1998)], pp. 1–98. DOI: 10.1142/9789812839657_0001,10.1142/9789814307505_0001. arXiv: hep-ph/9709356 [hep-ph].

[43] Geraldine Servant and Timothy M. P. Tait. "Is the lightest Kaluza-Klein particle a viable dark matter candidate?" In: *Nucl. Phys.* B650 (2003), pp. 391–419. DOI: 10.1016/S0550-3213(02)01012-X. arXiv: hep-ph/0206071 [hep-ph].

[44] R.D. Peccei and Helen Quinn. "CP Conservation in the Presence of Pseudoparticles". In: 38 (June 1977), pp. 1440–1443.

[45] Marco Drewes. "The Phenomenology of Right Handed Neutrinos". In: *Int. J. Mod. Phys.* E22 (2013), p. 1330019. DOI: 10.1142/S0218301313300191. arXiv: 1303.6912 [hep-ph].

[46] Lawrence J. Hall et al. "Freeze-in Production of FIMP dark matter". In: 2010 (Mar. 2010), pp. 1–33.

[47] Marco Cirelli. "Indirect Searches for Dark Matter: a status review". In: *Pramana* 79 (2012), pp. 1021–1043. DOI: 10.1007/s12043-012-0419-x. arXiv: 1202.1454 [hep-ph].

[48] Teresa Marrodán Undagoitia and Ludwig Rauch. "Dark matter direct-detection experiments". In: *J. Phys.* G43.1 (2016), p. 013001. DOI: 10.1088/0954-3899/43/1/013001. arXiv: 1509.08767 [physics.ins-det].

[49] Laura Baudis. "Direct dark matter detection: the next decade". In: *Phys. Dark Univ.* 1 (2012), pp. 94–108. DOI: 10.1016/j.dark.2012.10.006. arXiv: 1211.7222 [astro-ph.IM].

[50] Vasiliki A Mitsou. "Overview of searches for dark matter at the LHC". In: *Journal of Physics: Conference Series* 651.1 (2015), p. 012023. URL: http://stacks.iop.org/1742-6596/651/i=1/a=012023.

[51] A. Liam Fitzpatrick et al. "The Effective Field Theory of Dark Matter Direct Detection". In: *JCAP* 1302 (2013), p. 004. DOI: 10.1088/1475-7516/2013/02/004. arXiv: 1203.3542 [hep-ph].

[52] JiJi Fan, Matthew Reece, and Lian-Tao Wang. "Non-relativistic effective theory of dark matter direct detection". English. In: *Journal of Cosmology and Astroparticle Physics* 2010.11 (2010), p. 042.

[53] M. G. Aartsen et al. "Letter of Intent: The Precision IceCube Next Generation Upgrade (PINGU)". In: (2014). arXiv: 1401.2046 [physics.ins-det].

[54] M. G. Aartsen et al. "Search for annihilating dark matter in the Sun with 3 years of IceCube data". In: *Eur. Phys. J.* C77.3 (2017), p. 146. DOI: 10.1140/epjc/s10052-017-4689-9. arXiv: 1612.05949 [astro-ph.HE].

[55] A. Gould. "Resonant enhancements in weakly interacting massive particle capture by the earth". In: *Astrophysical Journal* 321 (Oct. 1987), pp. 571–585. DOI: 10.1086/165653.

[56] J. D. Lewin and P. F. Smith. "Review of mathematics, numerical factors, and corrections for dark matter experiments based on elastic nuclear recoil". In: *Astropart. Phys.* 6 (1996), pp. 87–112. DOI: 10.1016/S0927-6505(96)00047-3.

[57] Nikhil Anand, A. L. Fitzpatrick, and W. C. Haxton. "Model-independent WIMP Scattering Responses and Event Rates: A Mathematica Package for Experimental Analysis". English. In: (2013). eprint: https://arxiv.org/abs/1308.6288.

[58] Riccardo Catena and Bodo Schwabe. "Form factors for dark matter capture by the Sun in effective theories". In: *Journal of Cosmology and Astroparticle Physics* 2015.04 (2015), p. 042. URL: http://stacks.iop.org/1475-7516/2015/i=04/a=042.

[59] Paolo Gondolo et al. "DarkSUSY: A Numerical package for dark matter calculations in the MSSM". In: *Proceedings, 3rd International Workshop on The identification of dark matter (IDM 2000): York, UK, September 18-22, 2000.* 2000, pp. 318–323. arXiv: astro-ph/0012234 [astro-ph].

[60] Anne Schukraft. "A view of prompt atmospheric neutrinos with IceCube". In: *Nucl. Phys. Proc. Suppl.* 237-238 (2013), pp. 266–268. DOI: 10.1016/j.nuclphysbps.2013.04.105. arXiv: 1302.0127 [astro-ph.HE].

[61] M. Honda et al. "Atmospheric neutrino flux calculation using the NRLMSISE-00 atmospheric model". In: *Phys. Rev. D* 92 (2 2015), p. 023004. DOI: 10.1103/PhysRevD.92.023004. URL: https://link.aps.org/doi/10.1103/PhysRevD.92.023004.

[62] Rikard Enberg et al. "Prospects for higgsino-singlino dark matter detection at IceCube and PINGU". In: (2015). arXiv: 1506.05714 [hep-ph].

[63] Denis S. Robertson and Ivone F. M. Albuquerque. "Probing velocity dependent self-interacting dark matter with neutrino telescopes". In: *Journal of Cosmology and Astroparticle Physics* 2018.02 (2018), p. 056. URL: http://stacks.iop.org/1475-7516/2018/i=02/a=056.

[64] M. G. Aartsen et al. "Search for dark matter annihilations in the Sun with the 79-string IceCube detector". In: *Phys. Rev. Lett.* 110.13 (2013), p. 131302. DOI: 10.1103/PhysRevLett.110.131302. arXiv: 1212.4097 [astro-ph.HE].

[65] Glen Cowan et al. "Asymptotic formulae for likelihood-based tests of new physics". In: *Eur. Phys. J.* C71 (2011). [Erratum: Eur. Phys. J.C73,2501(2013)], p. 1554. DOI: 10.1140/epjc/s10052-011-1554-0,10.1140/epjc/s10052-013-2501-z. arXiv: 1007.1727 [physics.data-an].

[66] Ken Clark. "Status of the PINGU detector". In: *PoS* ICRC2015 (2016), p. 1174.

[67] Glen Cowan et al. "Asymptotic formulae for likelihood-based tests of new physics". In: *Eur. Phys. J.* C71 (2011). [Erratum: Eur. Phys. J.C73,2501(2013)], p. 1554. DOI: 10.1140/epjc/s10052-011-1554-0,10.1140/epjc/s10052-013-2501-z. arXiv: 1007.1727 [physics.data-an].

[68] Anne M Green. "Astrophysical uncertainties on the local dark matter distribution and direct detection experiments". In: *J. Phys.* G44.8 (2017), p. 084001. DOI: 10.1088/1361-6471/aa7819. arXiv: 1703.10102 [astro-ph.CO].

[69] Jonah Herzog-Arbeitman et al. "Empirical Determination of Dark Matter Velocities using Metal-Poor Stars". In: *Phys. Rev. Lett.* 120.4 (2018), p. 041102. DOI: 10.1103/PhysRevLett.120.041102. arXiv: 1704.04499 [astro-ph.GA].

[70] Riccardo Catena and Axel Widmark. "WIMP capture by the Sun in the effective theory of dark matter self-interactions". In: *JCAP* 1612.12 (2016), p. 016. DOI: 10.1088/1475-7516/2016/12/016. arXiv: 1609.04825 [astro-ph.CO].

[71] Joseph Bramante, Antonio Delgado, and Adam Martin. "Multiscatter stellar capture of dark matter". In: *Phys. Rev.* D96.6 (2017), p. 063002. DOI: 10.1103/PhysRevD.96.063002. arXiv: 1703.04043 [hep-ph].

[72] S Adrián-Martínez et al. "Letter of intent for KM3NeT 2.0". In: *Journal of Physics G: Nuclear and Particle Physics* 43.8 (2016), p. 084001. URL: http://stacks.iop.org/0954-3899/43/i=8/a=084001.

A

Appendix: isovector operators

In this appendix I include the sensitivity studies in the case of coupling constants with isovector coupling.

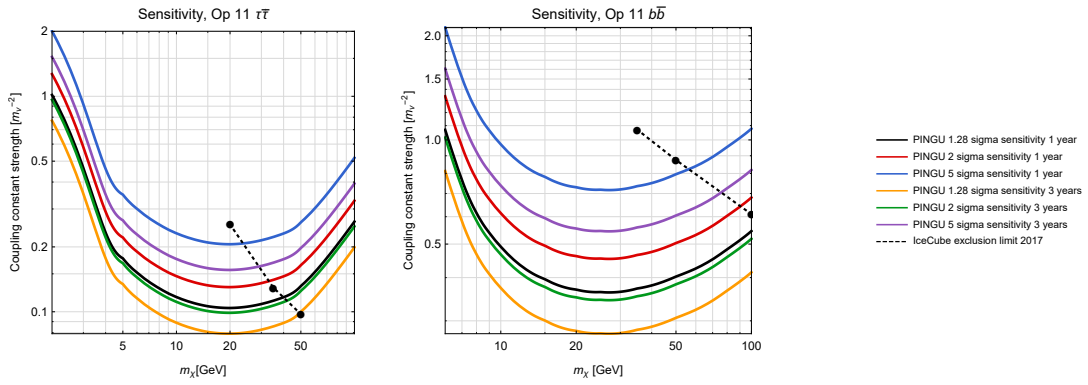

Figure A.1: Sensitivity studies for operator 1 for the $\tau\bar{\tau}$ channel (left) and $b\bar{b}$ (right).

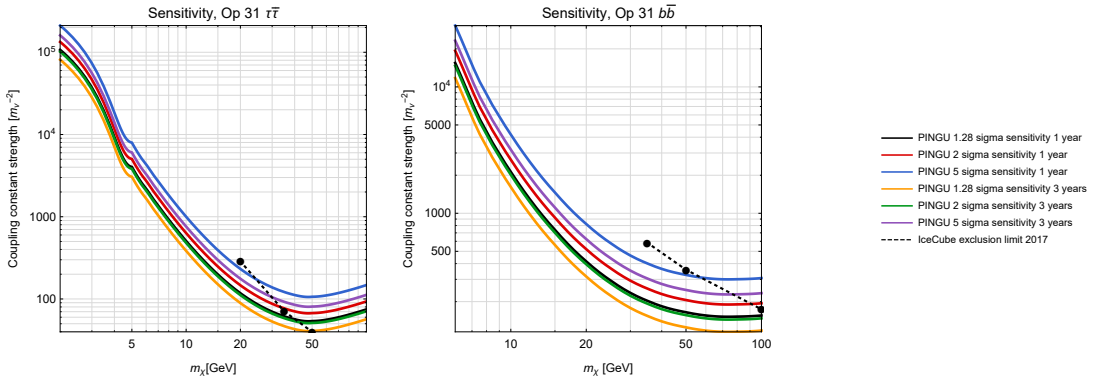

Figure A.2: Sensitivity studies for operator 3 for the $\tau\bar{\tau}$ channel (left) and $b\bar{b}$ (right).

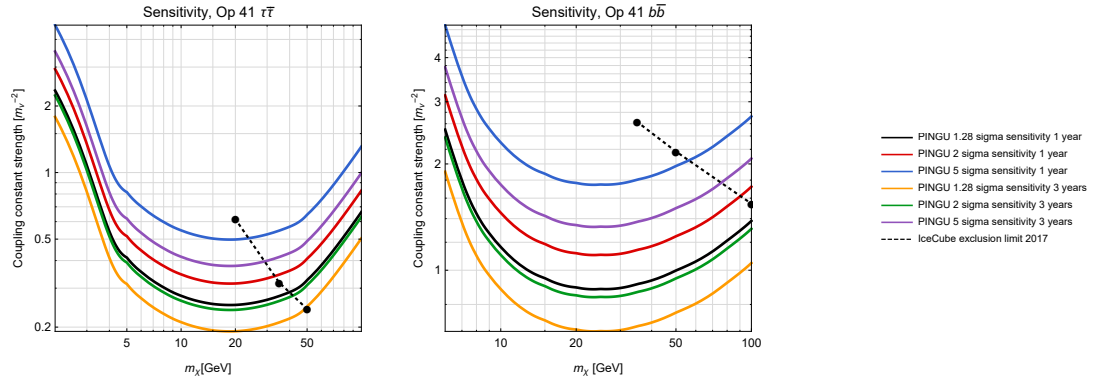

Figure A.3: Sensitivity studies for operator 4 for the $\tau\bar{\tau}$ channel (left) and $b\bar{b}$ (right).

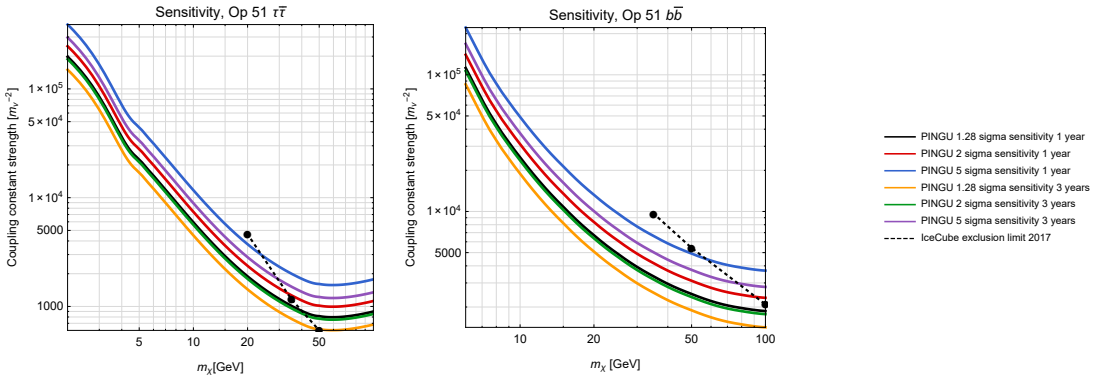

Figure A.4: Sensitivity studies for operator 5 for the $\tau\bar{\tau}$ channel (left) and $b\bar{b}$ (right).

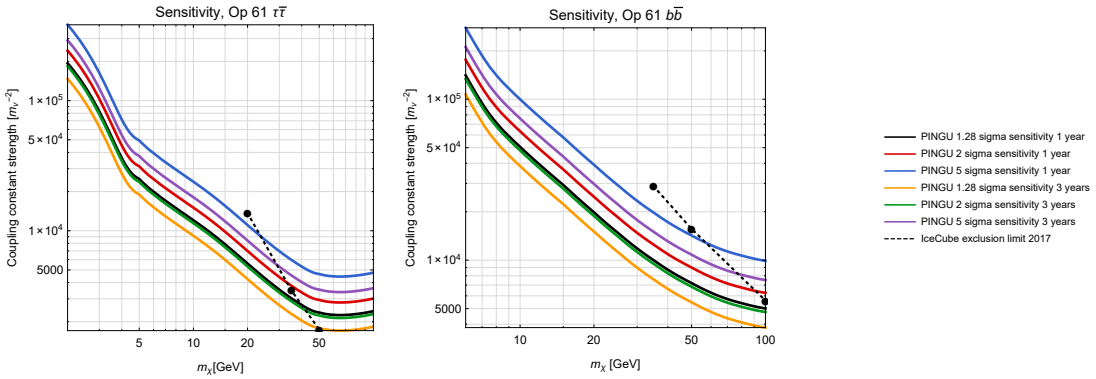

Figure A.5: Sensitivity studies for operator 6 for the $\tau\bar{\tau}$ channel (left) and $b\bar{b}$ (right).

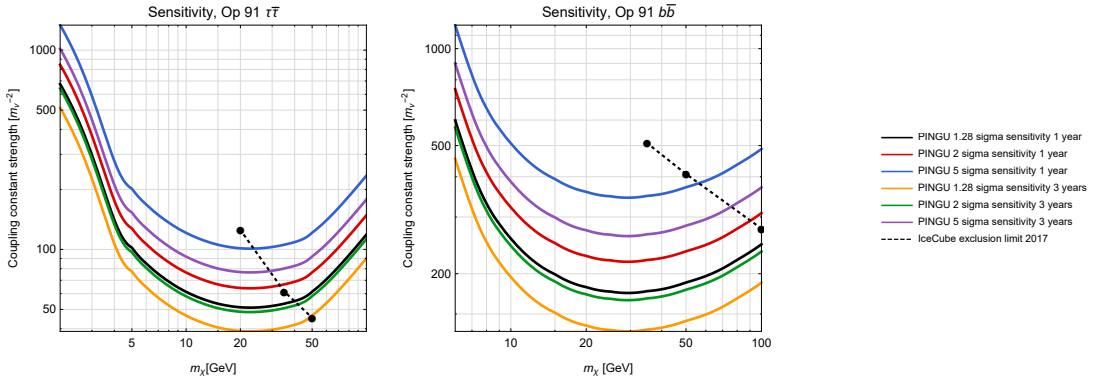

Figure A.8: Sensitivity studies for operator 9 for the $\tau\bar{\tau}$ channel (left) and $b\bar{b}$ (right).

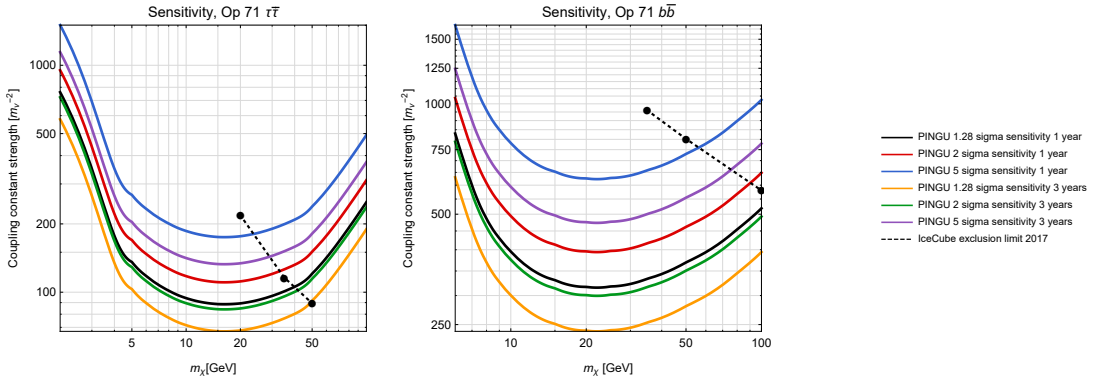

Figure A.6: Sensitivity studies for operator 7 for the $\tau\bar{\tau}$ channel (left) and $b\bar{b}$ (right).

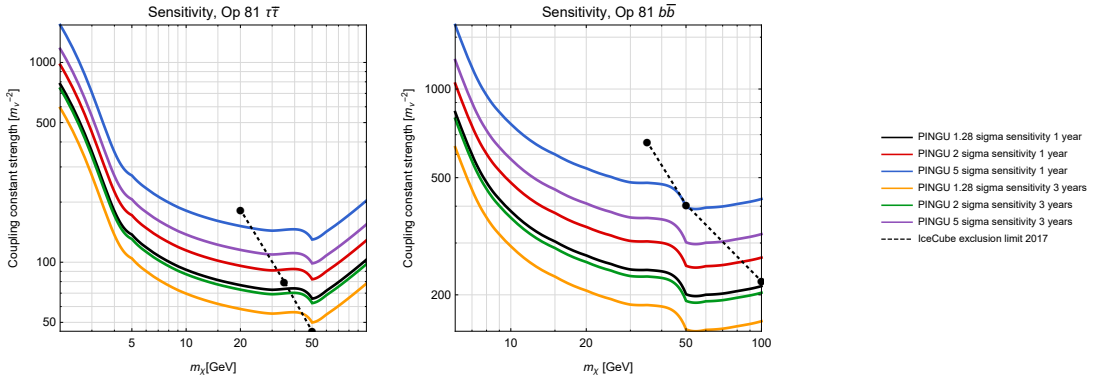

Figure A.7: Sensitivity studies for operator 8 for the $\tau\bar{\tau}$ channel (left) and $b\bar{b}$ (right).

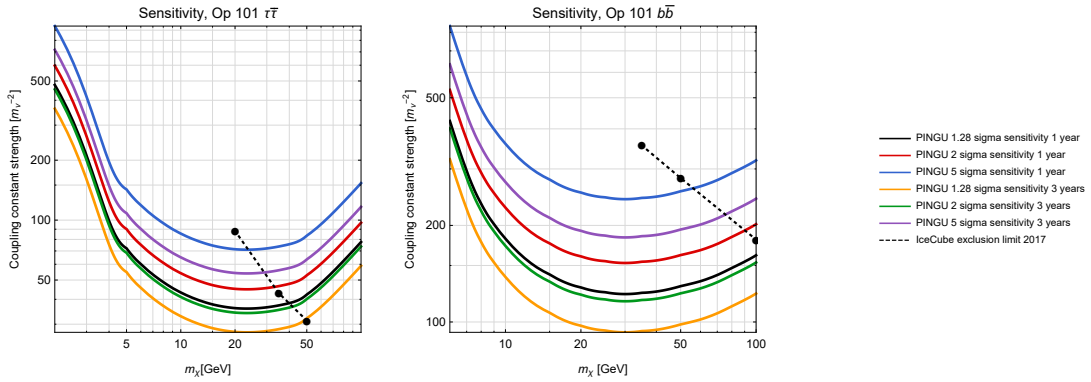

Figure A.9: Sensitivity studies for operator 10 for the $\tau\bar{\tau}$ channel (left) and $b\bar{b}$ (right).

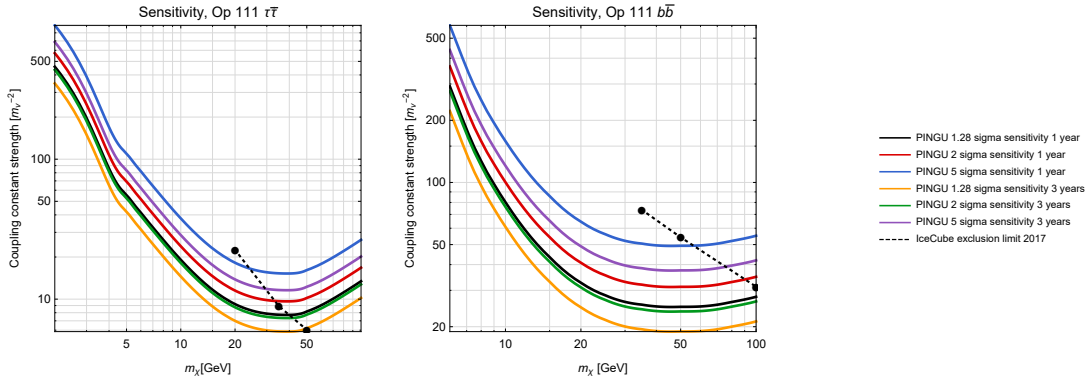

Figure A.10: Sensitivity studies for operator 11 for the $\tau\bar{\tau}$ channel (left) and $b\bar{b}$ (right).

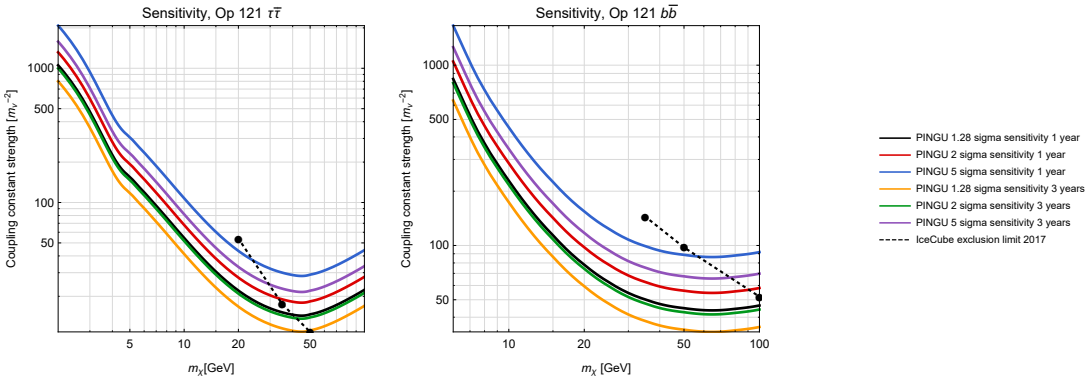

Figure A.11: Sensitivity studies for operator 12 for the $\tau\bar{\tau}$ channel (left) and $b\bar{b}$ (right).

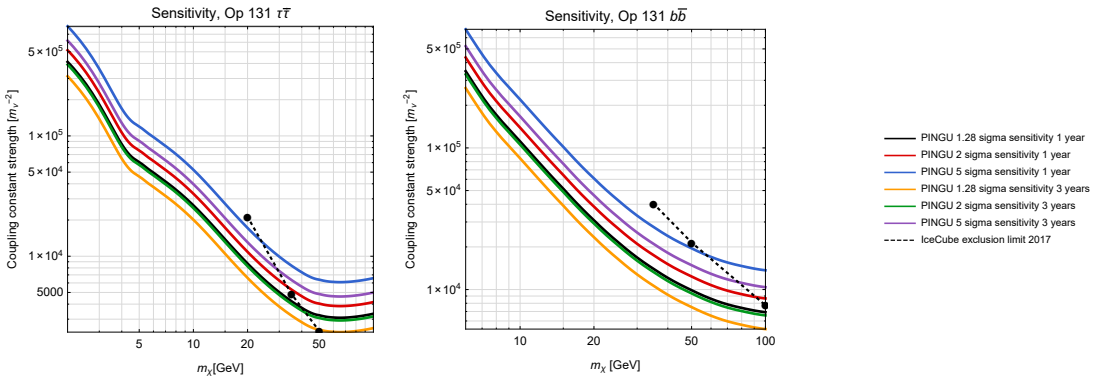

Figure A.12: Sensitivity studies for operator 13 for the $\tau\bar{\tau}$ channel (left) and $b\bar{b}$ (right).

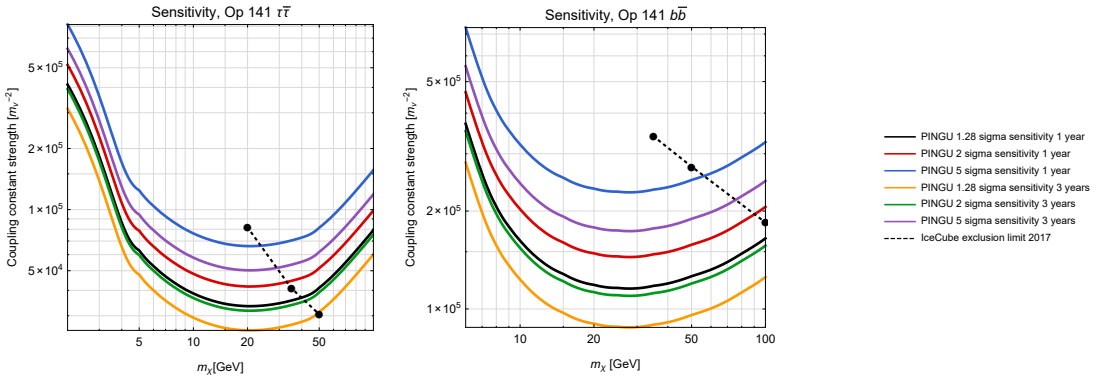

Figure A.13: Sensitivity studies for operator 14 for the $\tau\bar{\tau}$ channel (left) and $b\bar{b}$ (right).

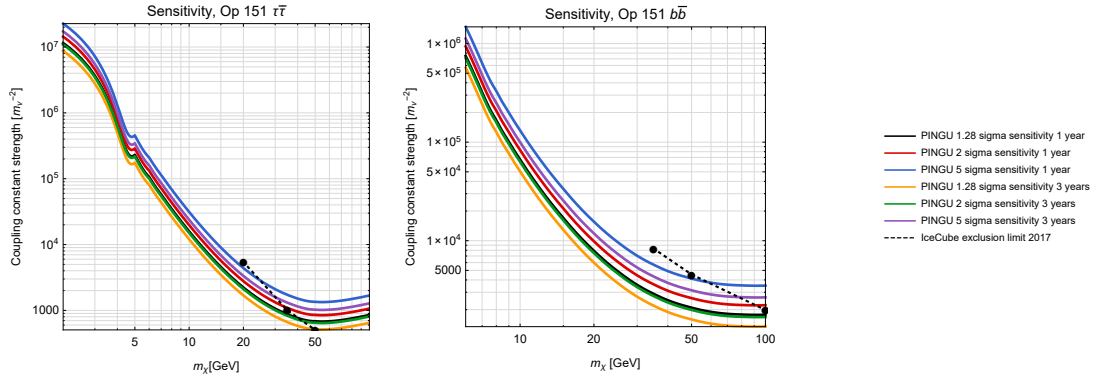

Figure A.14: Sensitivity studies for operator 15 for the $\tau\bar{\tau}$ channel (left) and $b\bar{b}$ (right).

B

Appendix: flowchart

I provide a flowchart over the calculations done in this thesis in order to calculate the signal N_s of neutrinos from dark matter annihilations. DMFF stands for the modified DMFORMFACTOR package.

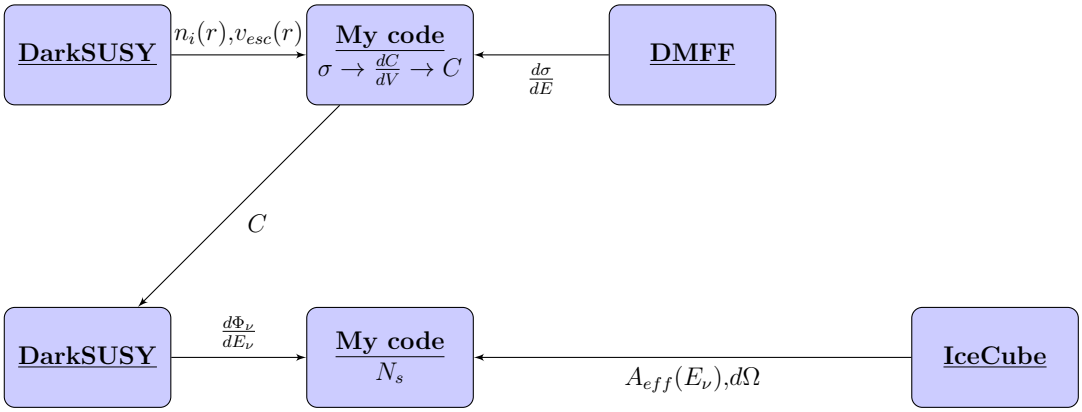

A similar flowchart is also provided in the case of background calculations.

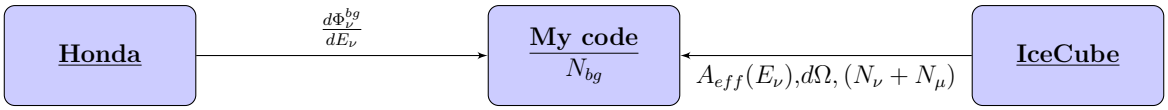

When the signal and background is calculated, eq.(3.43) can be solved in terms of the coupling constant c that results in the sought significance level.